Supplementary information to the paper

Pharmacological targeting of the Wdr5-MLL interaction in C/EBPα N-terminal leukemia

Florian Grebien[1,2*§], Masoud Vedadi[3,4*], Matthäus Getlik[5*], Roberto Giambruno[1], Amit Grover[6], Roberto Avellino[7], Anna Skucha[1], Sarah Vittori[1], Ekaterina Kuznetsova[3], David Smil[3], Dalia Barsyte-Lovejoy[3], Fengling Li[3], Gennadiy Poda[5,8], Matthieu Schapira[3,4], Hong Wu[3], Aiping Dong[3], Guillermo Senisterra[3], Alexey Stukalov[1], Kilian V. M. Huber[1], Andreas Schönegger[1], Richard Marcellus[5], Martin Bilban[9], Christoph Bock[1], Peter J. Brown[3], Johannes Zuber[10], Keiryn L. Bennett[1], Rima Al-awar[4,5], Ruud Delwel[7], Claus Nerlov[6], Cheryl H. Arrowsmith[3,11*§] and Giulio Superti-Furga[1*§]

[1] CeMM Research Center for Molecular Medicine of the Austrian Academy of Sciences, Vienna 1090, Austria

[2] Ludwig Boltzmann Institute for Cancer Research, Vienna 1090, Austria

[3] Structural Genomics Consortium, University of Toronto, Toronto, ON, M5G 1L7, Canada

[4] Department of Pharmacology and Toxicology, University of Toronto, Toronto, ON, M5S 1A8, Canada

[5] Drug Discovery Program, Ontario Institute for Cancer Research, Toronto, ON, M5G 0A3, Canada

[6] MRC Molecular Hematology Unit, Weatherall Institute of Molecular Medicine, Oxford OX3 9DS, United Kingdom

[7] Department of Hematology, Erasmus University Medical Center, Rotterdam 3015 GE, The Netherlands

[8] Leslie Dan Faculty of Pharmacy, University of Toronto, Toronto, ON, M5S 3M2, Canada

[9] Clinical Institute of Medical and Chemical Laboratory Diagnostics, Medical University Vienna, Vienna 1090, Austria

[10] Research Institute of Molecular Pathology (IMP), Vienna 1030, Austria

[11] Princess Margaret Cancer Centre and Department of Medical Biophysics, University of Toronto, Toronto, ON, M5G 2M9, Canada

* equal contribution

[§] correspondence to

Giulio Superti-Furga: gsuperti@cemm.oeaw.ac.at, phone: +43-1-40160-70001

Cheryl H Arrowsmith: carrow@uhnresearch.ca, phone: +1-416-946-0881

Florian Grebien: florian.grebien@lbicr.lbg.ac.at, phone: +43-1-40160-71240

Supplementary Results

Supplementary Tables 1-7

Supplementary Figures 1-16

Full, uncut gel images for Figures 1, 5 and Supplementary Figures 2, 5, 8 and 13.

Supplementary Table 1. Summary of LC-MS/MS data of C/EBPα p42 AP-MS experiments in FDCP-1 cells.

Gene_symbol	Description	SP_GN	PeptideCt_mock	Mean_PeptideCt_mock	PeptideCt_p42	Mean_PeptideCt_p42	SpectralCt_mock	Mean_SpectralCt_mock	SpectralCt_p42	Mean_SpectralCt_p42	Seqcov_mock	Mean_Seqcov_mock	Seqcov_p42	Mean_Seqcov_p42
Top2a	DNA topoisomerase 2-alpha	Top2a,Top2,Top-2	10	7.5	24	18.5	15	7.5	42	21	0.07	0.06	0.16	0.13
Hnrnpul2	Heterogeneous nuclear ribonucleoprotein U-like protein 2	Hnrnpul2,Hnrpul2,Manp	7	4.5	19	13.5	9	4.5	31	15.5	0.09	0.06	0.22	0.16
Nop56	Nucleolar protein 56	Nop56,Nol5a	4	2	15	12.5	4	2	31	15.5	0.07	0.04	0.26	0.22
Pdcd11	Protein RRP5 homolog	Pdcd11,Alg4,Kiaa0185	0	0	14	13	0	0	26	13	0	0	0.08	0.07
Myh9	Myosin-9	Myh9	0	0	14	10	0	0	22	11	0	0	0.08	0.06
Eif4a3	Eukaryotic initiation factor 4A-III	Eif4a3,Ddx48	8	4	13	11	8	4	22	11	0.17	0.09	0.23	0.2
Hp1bp3	Heterochromatin protein 1-binding protein 3	Hp1bp3	3	1.5	11	9	3	1.5	29	14.5	0.06	0.03	0.2	0.16
Nat10	N-acetyltransferase 10	Nat10,Kiaa1709	2	1	10	7.5	2	1	15	7.5	0.02	0.01	0.1	0.08
Rpn1	Dolichyl-diphosphooligosaccharide--protein glycosyltransf	Rpn1	2	1	9	7.5	2	1	15	7.5	0.04	0.02	0.16	0.14
Nop58	Nucleolar protein 58	Nop58,Nol5	2	1.5	9	5.5	5	2.5	16	8	0.04	0.03	0.18	0.11
Nol6	Nucleolar protein 6	Nol6	0	0	9	5.5	0	0	12	6	0	0	0.07	0.05
Acin1	Apoptotic chromatin condensation inducer in the nucleus	Acin1,Acinus	2	1	7	5	2	1	14	7	0.02	0.01	0.06	0.04
Ddx18	ATP-dependent RNA helicase DDX18	Ddx18	2	1.5	8	7.5	3	1.5	19	9.5	0.03	0.02	0.12	0.12
NA	rat CEBPA Strep-HA protein	NA	0	0	7	6	0	0	19	9.5	0	0	0.16	0.14
Matr3	Matrin-3	Matr3	0	0	7	5.5	0	0	11	5.5	0	0	0.09	0.07
Noc2l	Nucleolar complex protein 2 homolog	Noc2l	0	0	7	5.5	0	0	13	6.5	0	0	0.07	0.06
Nup93	Nuclear pore complex protein Nup93	Nup93,Kiaa0095,Cip4	0	0	7	4.5	0	0	9	4.5	0	0	0.09	0.06
Mogs	Mannosyl-oligosaccharide glucosidase	Mogs,Gcs1	0	0	6	3.5	0	0	7	3.5	0	0	0.07	0.04
Zfr	Zinc finger RNA-binding protein	Zfr	1	0.5	6	5.5	1	0.5	13	6.5	0.02	0.01	0.07	0.06
Ddx47	Probable ATP-dependent RNA helicase DDX47	Ddx47	1	0.5	5	3	1	0.5	6	3	0.02	0.01	0.12	0.07
Baz1a	Bromodomain adjacent to zinc finger domain protein 1A	Baz1a,Cbp146	1	0.5	6	4.5	1	0.5	14	7	0.01	0	0.04	0.03
Lmnb1	Lamin-B1	Lmnb1	2	1	6	5.5	2	1	11	5.5	0.04	0.02	0.11	0.1
Srsf5	Serine/arginine-rich splicing factor 5	Srsf5,Sfrs5,Hrs	2	2	5	4	7	3.5	21	10.5	0.09	0.09	0.17	0.14
Mta2	Metastasis-associated protein MTA2	Mta2,Mta1l1	0	0	5	3.5	0	0	7	3.5	0	0	0.07	0.05
Hdac2	Histone deacetylase 2	Hdac2,Yy1bp	3	2	5	4.5	4	2	9	4.5	0.07	0.04	0.09	0.09
Hdac1	Histone deacetylase 1	Hdac1	0	0	5	4	0	0	8	4	0	0	0.1	0.08
Snrnp70	U1 small nuclear ribonucleoprotein 70 kDa	Snrnp70,Snrp70	0	0	5	3.5	0	0	8	4	0	0	0.1	0.07
Rbm39	RNA-binding protein 39	Rbm39,Rnpc2,Caper	0	0	5	3.5	0	0	8	4	0	0	0.11	0.06
Lbr	Lamin-B receptor	Lbr	0	0	4	2	0	0	4	2	0	0	0.06	0.03
Rpn2	Dolichyl-diphosphooligosaccharide--protein glycosyltransf	Rpn2	0	0	4	2.5	0	0	5	2.5	0	0	0.08	0.05
Usp39	U4/U6.U5 tri-snRNP-associated protein 2	Usp39	0	0	4	2	0	0	4	2	0	0	0.07	0.04
Mcm4	DNA replication licensing factor MCM4	Mcm4,Cdc21,Mcmd4	0	0	4	2	0	0	4	2	0	0	0.05	0.02
Rrp1b	Ribosomal RNA processing protein 1 homolog B	Rrp1b	1	0.5	4	4	1	0.5	9	4.5	0.02	0.01	0.07	0.07
Urb1	Nucleolar pre-ribosomal-associated protein 1	Urb1,Npa1,Kiaa0539	0	0	4	3.5	0	0	7	3.5	0	0	0.02	0.02
Pnn	Pinin	Pnn	0	0	4	3.5	0	0	7	3.5	0	0	0.06	0.05
Ints7	Integrator complex subunit 7	Ints7	0	0	4	2	0	0	4	2	0	0	0.05	0.02
Sap18	Histone deacetylase complex subunit SAP18	Sap18	0	0	4	2	0	0	4	2	0	0	0.18	0.09
Smarcd1	SWI/SNF-related matrix-associated actin-dependent regu	Smarcd1,D15Kz1,Baf60a	0	0	4	2.5	0	0	5	2.5	0	0	0.09	0.05
Cebpz	CCAAT/enhancer-binding protein zeta	Cebpz,Cebpa-rs1,Cbf2	0	0	4	2	0	0	4	2	0	0	0.04	0.02
Srsf3	Serine/arginine-rich splicing factor 3	Srsf3,X16,Sfrs3,Srp20	1	0.5	2	2	1	0.5	4	2	0.09	0.04	0.07	0.07
Nup160	Nuclear pore complex protein Nup160	Nup160,Gtl1-13,Kiaa0197	0	0	3	3	0	0	6	3	0	0	0.02	0.02
Lig3	DNA ligase 3	Lig3	1	0.5	3	2	1	0.5	4	2	0.01	0	0.03	0.02
Rps25	40S ribosomal protein S25	Rps25	0	0	3	2	0	0	4	2	0	0	0.21	0.14
Kiaa0020	Pumilio domain-containing protein KIAA0020	Kiaa0020,D19Bwg1357e	0	0	3	2.5	0	0	5	2.5	0	0	0.04	0.04
Sin3a	Paired amphipathic helix protein Sin3a	Sin3a,Kiaa4126	1	0.5	3	2.5	1	0.5	6	3	0.01	0	0.03	0.02
Gnb2	Guanine nucleotide-binding protein G(I)/G(S)/G(T) subuni	Gnb2	0	0	3	2	0	0	4	2	0	0	0.1	0.06
Stag1	Cohesin subunit SA-1	Stag1,Sa1	1	0.5	3	2.5	1	0.5	5	2.5	0.01	0	0.03	0.02
Rrp12	RRP12-like protein	Rrp12,Kiaa0690	0	0	3	2.5	0	0	5	2.5	0	0	0.02	0.02
Ewsr1	RNA-binding protein EWS	Ewsr1,Ewsh,Ews	1	1	3	2.5	4	2	6	3	0.02	0.02	0.05	0.05
Polr2a	DNA-directed RNA polymerase II subunit RPB1	Polr2a,Rpii215,Rpo2-1	0	0	3	2.5	0	0	5	2.5	0	0	0.01	0.01
Eif2s1	Eukaryotic translation initiation factor 2 subunit 1	Eif2s1,Eif2a	0	0	3	2	0	0	4	2	0	0	0.09	0.07
Nol10	Nucleolar protein 10	Nol10,Gm67	0	0	2	2	0	0	4	2	0	0	0.03	0.03
Rps9	40S ribosomal protein S9	Rps9	0	0	2	2	0	0	4	2	0	0	0.09	0.09
H2afz	Histone H2A.Z	H2afz,H2az	0	0	2	2	0	0	4	2	0	0	0.12	0.12
Ftsj3	Putative rRNA methyltransferase 3	Ftsj3	0	0	2	2	0	0	5	2.5	0	0	0.02	0.02
Ddx54	ATP-dependent RNA helicase DDX54	Ddx54	0	0	2	2	0	0	4	2	0	0	0.02	0.02
Rps14	40S ribosomal protein S14	Rps14	0	0	2	2	0	0	4	2	0	0	0.16	0.16
Ddit3	DNA damage-inducible transcript 3 protein	Ddit3,Gadd153,Chop,Chop	0	0	2	2	0	0	7	3.5	0	0	0.07	0.07
Ppp2r1a	Serine/threonine-protein phosphatase 2A 65 kDa regulate	Ppp2r1a	0	0	2	2	0	0	4	2	0	0	0.04	0.04
NA	Cell cycle regulator Mat89Bb homolog	NA	0	0	2	2	0	0	4	2	0	0	0.03	0.03
Rpl27	60S ribosomal protein L27	Rpl27	1	0.5	2	2	1	0.5	4	2	0.07	0.03	0.12	0.12
Myl6	Myosin light polypeptide 6	Myl6,Myln	1	0.5	2	2	1	0.5	4	2	0.09	0.04	0.15	0.15
Kpnb1	Importin subunit beta-1	Kpnb1,Impnb	0	0	2	2	0	0	4	2	0	0	0.02	0.02
Hdgfrp2	Hepatoma-derived growth factor-related protein 2	Hdgfrp2	0	0	2	2	0	0	4	2	0	0	0.03	0.03

Supplementary Table 2. Summary of LC-MS/MS data of C/EBPα p30 AP-MS experiments in FDCP-1 cells.

Gene_symbol	Description	SP_GN	PeptideCt_mock	Mean_PeptideCt_mock	PeptideCt_p30	Mean_PeptideCt_p30	SpectralCt_mock	Mean_SpectralCt_mock	SpectralCt_p30	Mean_SpectralCt_p30	Seqcov_mock	Mean_Seqcov_mock	Seqcov_p30	Mean_Seqcov_p30
Sptbn1	Spectrin beta chain, brain 1	Sptbn1,Sptb2,Elf,Spnb-2,Spnb	3	1	23	12.5	3	1	25	12.5	0.02	0.01	0.11	0.06
Top1	DNA topoisomerase 1	Top1,Top-1	13	7.33	22	18	31	10.33	63	31.5	0.17	0.09	0.28	0.24
Hnrnpm	Heterogeneous nuclear ribonucleoprotein M	Hnrnpm,Hnrpm	8	4.33	19	12	15	5	40	20	0.11	0.06	0.28	0.18
Sptan1	Spectrin alpha chain, brain	Sptan1,Spta2,Spna2	3	1	18	9	3	1	19	9.5	0.01	0	0.08	0.04
Hspa5	78 kDa glucose-regulated protein	Hspa5,Grp78	4	2.33	12	8.5	13	4.33	24	12	0.08	0.05	0.25	0.18
Ddx18	ATP-dependent RNA helicase DDX18	Ddx18	3	1.33	12	7.5	4	1.33	18	9	0.05	0.02	0.2	0.12
Hp1bp3	Heterochromatin protein 1-binding protein 3	Hp1bp3	5	1.67	9	7.5	5	1.67	22	11	0.11	0.04	0.17	0.14
Rps3	40S ribosomal protein S3	Rps3	2	1.33	10	7	4	1.33	18	9	0.11	0.07	0.47	0.32
Ints7	Integrator complex subunit 7	Ints7	0	0	10	5	0	0	10	5	0	0	0.13	0.06
Rps4x	40S ribosomal protein S4, X isoform	Rps4x,Rps4	5	1.67	9	6	5	1.67	16	8	0.21	0.07	0.33	0.24
Vcp	Transitional endoplasmic reticulum ATPase	Vcp	4	1.33	7	6	4	1.33	13	6.5	0.07	0.02	0.1	0.09
Thoc5	THO complex subunit 5 homolog	Thoc5,Kiaa0983,Fmip	2	1.33	8	5	4	1.33	12	6	0.03	0.02	0.13	0.08
Smu1	WD40 repeat-containing protein SMU1	Smu1	2	1.67	6	4	5	1.67	14	7	0.05	0.05	0.16	0.11
Thoc1	THO complex subunit 1	Thoc1,Hpr1	3	1	7	6	3	1	12	6	0.05	0.02	0.13	0.11
Nup93	Nuclear pore complex protein Nup93	Nup93,Kiaa0095,Cip4	0	0	7	4	0	0	8	4	0	0	0.1	0.06
Srsf5	Serine/arginine-rich splicing factor 5	Srsf5,Sfrs5,Hrs	2	2	6	4	11	3.67	20	10	0.09	0.09	0.23	0.16
D1Pas1	Putative ATP-dependent RNA helicase Pl10	D1Pas1,Pl10	1	0.33	6	4.5	1	0.33	11	5.5	0.02	0.01	0.12	0.08
Ppp1ca	Serine/threonine-protein phosphatase PP1-alpha catalytic sub	Ppp1ca,Ppp1a	1	0.33	6	3	1	0.33	7	3.5	0.04	0.01	0.24	0.12
Ogt	UDP-N-acetylglucosamine--peptide N-acetylglucosaminyltran	Ogt	0	0	6	3.5	0	0	7	3.5	0	0	0.06	0.03
Mcm7	DNA replication licensing factor MCM7	Mcm7,Cdc47,Mcmd7	1	0.67	6	4	2	0.67	8	4	0.02	0.01	0.1	0.07
Rfc2	Replication factor C subunit 2	Rfc2	1	0.33	6	4	1	0.33	8	4	0.04	0.01	0.23	0.16
Mcm4	DNA replication licensing factor MCM4	Mcm4,Cdc21,Mcmd4	0	0	5	2.5	0	0	5	2.5	0	0	0.07	0.04
Zfr	Zinc finger RNA-binding protein	Zfr	1	0.33	5	2.5	1	0.33	5	2.5	0.02	0.01	0.06	0.03
Ddx47	Probable ATP-dependent RNA helicase DDX47	Ddx47	1	0.33	5	3.5	1	0.33	7	3.5	0.02	0.01	0.13	0.09
Gzmb	Granzyme B(G,H)	Gzmb,Ctla1,Ctla-1	0	0	5	2.5	0	0	6	3	0	0	0.15	0.08
Nup160	Nuclear pore complex protein Nup160	Nup160,Gtl1-13,Kiaa0197	0	0	4	2	0	0	4	2	0	0	0.03	0.01
Dbt	Lipoamide acyltransferase component of branched-chain alph	Dbt	0	0	4	2	0	0	4	2	0	0	0.09	0.04
Rfc3	Replication factor C subunit 3	Rfc3	0	0	4	2	0	0	4	2	0	0	0.13	0.06
Prpf4	U4/U6 small nuclear ribonucleoprotein Prp4	Prpf4	0	0	4	2.5	0	0	5	2.5	0	0	0.07	0.06
NA	rat CEBPA Strep-HA protein	NA	0	0	4	3.5	0	0	12	6	0	0	0.09	0.08
Safb2	Scaffold attachment factor B2	Safb2	1	0.33	4	2	1	0.33	6	3	0.01	0	0.06	0.03
Smarcd2	SWI/SNF-related matrix-associated actin-dependent regulator	Smarcd2,Baf60b	0	0	4	2	0	0	4	2	0	0	0.1	0.05
Nup107	Nuclear pore complex protein Nup107	Nup107	0	0	4	3	0	0	6	3	0	0	0.05	0.03
Wtap	Pre-mRNA-splicing regulator WTAP	Wtap	0	0	4	2	0	0	4	2	0	0	0.13	0.06
Med23	Mediator of RNA polymerase II transcription subunit 23	Med23,Kiaa1216,Crsp3,Sur2	0	0	4	2	0	0	4	2	0	0	0.03	0.02
NA	Ig kappa chain C region	NA	0	0	4	2	0	0	16	8	0	0	0.39	0.19
Ppp1cb	Serine/threonine-protein phosphatase PP1-beta catalytic subu	Ppp1cb	1	0.33	4	2	1	0.33	4	2	0.04	0.01	0.17	0.08
Ncoa5	Nuclear receptor coactivator 5	Ncoa5	0	0	4	2.5	0	0	7	3.5	0	0	0.11	0.07
Bub3	Mitotic checkpoint protein BUB3	Bub3	0	0	4	2	0	0	4	2	0	0	0.16	0.08
Tcerg1	Transcription elongation regulator 1	Tcerg1,Taf2s	0	0	4	2.5	0	0	5	2.5	0	0	0.04	0.02
Kpnb1	Importin subunit beta-1	Kpnb1,Impnb	0	0	4	2	0	0	4	2	0	0	0.06	0.03
Wdr5	WD repeat-containing protein 5	Wdr5,Big,Big3	1	0.33	4	2.5	1	0.33	5	2.5	0.04	0.01	0.16	0.1
Rad21	Double-strand-break repair protein rad21 homolog	Rad21,Hr21	1	0.33	4	3.5	1	0.33	7	3.5	0.02	0.01	0.08	0.07
Eif2s1	Eukaryotic translation initiation factor 2 subunit 1	Eif2s1,Eif2a	1	0.33	3	2	1	0.33	4	2	0.05	0.02	0.12	0.08
Rfc4	Replication factor C subunit 4	Rfc4	1	0.33	3	2	1	0.33	4	2	0.03	0.01	0.08	0.05
Matr3	Matrin-3	Matr3	1	0.33	3	2.5	1	0.33	8	4	0.02	0.01	0.05	0.04
Rnps1	RNA-binding protein with serine-rich domain 1	Rnps1	1	1	3	2	3	1	5	2.5	0.05	0.05	0.11	0.08
Nxf1	Nuclear RNA export factor 1	Nxf1,Tap	0	0	3	2.5	0	0	6	3	0	0	0.06	0.05
Ddx1	ATP-dependent RNA helicase DDX1	Ddx1	1	0.67	3	2	2	0.67	7	3.5	0.01	0.01	0.04	0.03
Stag1	Cohesin subunit SA-1	Stag1,Sa1	1	0.33	3	2	1	0.33	4	2	0.01	0	0.03	0.02
Pycr2	Pyrroline-5-carboxylate reductase 2	Pycr2	0	0	3	2	0	0	4	2	0	0	0.13	0.08
Rpl27	60S ribosomal protein L27	Rpl27	1	0.33	2	2	1	0.33	5	2.5	0.07	0.02	0.12	0.12

Supplementary Table 3. Selectivity of OICR-9429 against 215 protein kinases and a panel of GPCRs, ion channels and transporters. Activity assays were performed at CEREP (www.cerep.fr/Cerep/Users/index.asp) at 1 µM. As none of these kinases showed >50% inhibition, IC_{50} values were assumed to be higher than 1 µM, and thus OICR-9429 is >20-fold selective for all kinases measured.

Protein	Act (%)	Protein	Act (%)	Protein	Act (%)	Protein	Act (%)
Abl kinase	107	FGFR1 kinase	96	NEK6	96	TTK	99
Ack	100	FGFR2 kinase	105	NEK7	92	TXK	94
ALK	99	FGFR3 kinase	105	NIK	104	Tyk2 (JTK1)	102
Akt1/PKBalpha	115	FGFR4 kinase	112	NuaK1 (ARK5)	105	Tyro3 /Sky kinase	105
Akt2/PKBbeta	94	Fgr kinase	102	p38alpha kinase	97	ULK1	92
Akt3/PKBgamma	107	FLT-1 kinase (VEGFR1)	110	p38delta kinase	106	Wee1 kinase	100
ALK4 (ACVR1B)	91	FLT-3 kinase	122	p70S6K	99	WNK2	94
AMPKalpha	97	FLT-4 kinase (VEGFR3)	105	p70S6Kbeta	105	WNK3	103
Arg kinase	93	Fms/CSFR kinase	130	PAK2	110	WNK4	99
ASK1	100	FRK	111	PAK4	102	Yes kinase	115
AurA/Aur2 kinase	104	Fyn kinase	117	PASK	94	ZAP70 kinase	103
AurC/Aur3 kinase	81	GCK (MAP4K2)	102	PCTAIRE1 kinase	102	A1 (h) (antagonist radioligand)	100
Axl kinase	98	GRK2 (ADRBK1)	110	PDGFRalpha kinase	101	A2A (h) (agonist radioligand)	101
BMPR1A (ALK3)	102	GRK3 /BARK2 (ADRBK2)	95	PDGFRbeta kinase	99	A3 (h) (agonist radioligand)	95
Brk	107	GSK3alpha	97	PDK1	99	alpha 1 (non-selective) (antagonist radioligand)	99
BRSK1	91	GSK3beta	104	PEK (EIF2AK3)	97	alpha 2 (non-selective) (antagonist radioligand)	98
CaMK1alpha	96	HER2/ErbB2 kinase	102	PhKgamma 1	116	beta 1 (h) (agonist radioligand)	88
CaMK1delta	103	HGK (MAP4K4)	96	PhKgamma 2	110	beta 2 (h) (agonist radioligand)	93
CaMK2alpha	111	HIPK2	100	Pim1 kinase	96	AT1 (h) (antagonist radioligand)	118
CaMK4	99	HIPK4	93	Pim2 kinase	101	BZD (central) (agonist radioligand)	126
CDC2/CDK1 (cycB)	105	IGF1R kinase	107	PKA	104	B2 (h) (agonist radioligand)	104
CDC7 /ASK	94	IKKalpha	103	PKCalpha	110	CB1 (h) (agonist radioligand)	95
CDK2 (cycA)	104	IKKbeta	105	PKCbeta 1	98	CCK1 (CCKA) (h) (agonist radioligand)	125
CDK3 (cycE1)	83	IKKepsilon (IKBKE)	89	PKCbeta 2	98	D1 (h) (antagonist radioligand)	100
CDK4 (cycD1)	102	IRAK1	99	PKCgamma	97	D2S (h) (antagonist radioligand)	97
CDK5 /p35	102	IRAK4	99	PKCdelta	101	ETA (h) (agonist radioligand)	104
CDK6 (cycD3)	114	IRK (InsR)	80	PKCzeta	116	GABA (non-selective) (agonist radioligand)	91
CDK7 /MAT1 (cycH)	82	IRR kinase	112	PKCeta	91	GAL2 (h) (agonist radioligand)	108
CDK8 (cycC)	105	ITK	107	PKCtheta	98	CXCR2 (IL-8B) (h) (agonist radioligand)	97
CDK9 (cycT1)	98	JAK1	101	PKD2	104	CCR1 (h) (agonist radioligand)	106
CHK1	93	JAK2	103	PKD3	95	H1 (h) (antagonist radioligand)	106
CHK2	101	JAK3	103	PKG1alpha	105	H2 (h) (antagonist radioligand)	87
CK1alpha	100	JNK1	88	PKG1beta	101	MC4 (h) (agonist radioligand)	86
CK2 (casein kinase 2)	103	JNK2	87	PKG2	89	MT1 (ML1A) (h) (agonist radioligand)	98
c-kit kinase	73	JNK3	102	PKN1	96	M1 (h) (antagonist radioligand)	98
CLK1	99	KDR kinase (VEGFR2)	99	PKN2	93	M2 (h) (antagonist radioligand)	92
CLK2	105	Lck kinase	112	PKR (EIF2AK2)	109	M3 (h) (antagonist radioligand)	83
c-Met kinase	90	LIMK1	103	PLK1	99	NK2 (h) (agonist radioligand)	99
COT kinase (MAP3K8)	113	LTK	105	PLK2	98	NK3 (h) (antagonist radioligand)	99
CRIK	93	Lyn A kinase	107	PLK4	97	Y1 (h) (agonist radioligand)	115
DAPK1	94	Lyn B kinase	100	PRKX	103	Y2 (h) (agonist radioligand)	127
DAPK2	102	MEK5 (MAP2K5)	100	PYK2	104	NTS1 (NT1) (h) (agonist radioligand)	85
DCAMKL1	114	MEKK4 (MAP3K4)	101	B-Raf kinase	101	delta 2 (DOP) (h) (agonist radioligand)	103
DCAMKL2	114	MAPKAPK2	114	RAF-1 kinase	95	kappa (KOP) (agonist radioligand)	102
DDR2 kinase	110	MAPKAPK5 (PRAK)	78	Ret kinase	104	mu (MOP) (h) (agonist radioligand)	103
DLK1 (MAP3K12)	102	MARK1	104	RIPK2	98	NOP (ORL1) (h) (agonist radioligand)	99
DRAK1	101	MARK2	109	ROCK1	101	EP4 (h) (agonist radioligand)	113
DYRK1a	99	MARK3	104	ROCK2	100	5-HT1A (h) (agonist radioligand)	109
DYRK2	87	MARK4	100	Ron kinase	106	5-HT1B (antagonist radioligand)	118
DYRK4	92	MEKK3 (MAP3K3)	97	RSK1	110	5-HT2A (h) (antagonist radioligand)	97
EGFR kinase	100	NIM1 kinase (MGC42105)	102	RSK2	103	5-HT2B (h) (agonist radioligand)	72
EphA1 kinase	88	MINK	107	RSK3	115	5-HT3 (h) (antagonist radioligand)	91
EphA2 kinase	89	MLK1	96	SGK1	100	5-HT5a (h) (agonist radioligand)	110
EphA3 kinase	105	MNK1	94	SGK3	100	5-HT6 (h) (agonist radioligand)	94
EphA4 kinase	93	MLK2 (MAP3K10)	98	SIK	98	5-HT7 (h) (agonist radioligand)	67
EphA5 kinase	97	MNK2	91	Src kinase	86	sst (non-selective) (agonist radioligand)	108
EphA7 kinase	98	MOS kinase	108	STK33	92	VPAC1 (VIP1) (h) (agonist radioligand)	112
EphB1 kinase	118	MSK2	114	Syk	100	V1a (h) (agonist radioligand)	101
EphB2 kinase	105	MST1 kinase (STK4)	97	TAK1-TAB1 (MAP3K7)	105	Ca2+ channel (L, verapamil site) (antagonist radioligand)	101
EphB3 kinase	76	MST2 kinase	100	TAOK2 (TAO1)	103	KV channel (antagonist radioligand)	121
EphB4 kinase	106	MST3 kinase	95	TBK1	100	SKCa channel (antagonist radioligand)	105
ERK1	112	MST4 kinase	102	TIE2 kinase	103	Na+ channel (site 2) (antagonist radioligand)	94
ERK2 (P42mapk)	100	MusK	105	Tnk1	95	Cl- channel (GABA-gated) (antagonist radioligand)	110
ERK5 (MAPK7)	92	MYT1 kinase	88	TRKA	97	norepinephrine transporter (h) (antagonist radioligand)	94
FAK	106	NDR1 kinase	98	TRKB	96	dopamine transporter (h) (antagonist radioligand)	105
Fes kinase	106	NEK2	100	TRKC	114	5-HT transporter (h) (antagonist radioligand)	108
Fer kinase	103	NEK4	100	TSSK1	93		

Supplementary Table 4. Selectivity of OICR-9429 against 22 protein methyltransferases and DNMT1. .As the lowest activity was 79% for all PMTs tested at 50 µM, IC_{50} values were assumed to be higher than 50 µM, and thus OICR-9429 is >1000-fold selective for all PMTs measured.

Protein	Activity (%) at 50 µM
SMYD2	99
G9a	92
EHMT1	111
SUV39H2	106
SETDB1	89
SETD7	109
SETD8	103
SUV420H1	113
SUV420H2	106
PRMT1	97
PRMT3	100
PRMT5	100
PRMT6	95
PRMT8	97
PRMD9	98
EZH1	101
EZH2	111
NSD1	111
NSD2	79
NSD3	122
SETD2	119
DOT1L	94
DNMT1	102

Supplementary Table 5. Crystallography data and refinement statistics

	WDR5+OICR-9429
Data collection	
Space group	P1
Cell dimensions	
a, *b*, *c* (Å)	46.8, 56.6, 64.7
a, b, g (°)	71.5, 88.9, 65.4
Resolution (Å)	50.00-1.50(1.53-1.50) *
R_{sym} or R_{merge}	6.7(39.2)
I / s I	39.5(6.0)
Completeness (%)	94.8(70.2)
Redundancy	3.7(3.7)
Refinement	
Resolution (Å)	50.00-1.50
No. reflections	85825
R_{work} / R_{free}	19.5/22.7
No. atoms	
Protein	4699
Ligand/ion	72
Water	332
B-factors	
Protein	15.4
Ligand/ion	14.4
Water	23.5
R.m.s. deviations	
Bond lengths (Å)	0.009
Bond angles (°)	1.373

Supplementary Table 6. qPCR primers used in this study

Wdr5	Forward Reverse	GGTCATCAGATTCTAACCTCCT GGTTGAAATGAACGGCTGAG
C3ar1	Forward Reverse	ATGATCCTGAGTTCCCTTTACC TCCCAATAGACAAGTGAGACC
Ccl9	Forward Reverse	CCCACTAAGAAGATGAAGCCT CTTGCTGATAAAGATGATGCCC
Lilrb3	Forward Reverse	AAGGCTCTCATTGGAGTGTC CTGAAGCATATAGGCTTTCTTCC
Lyz2	Forward Reverse	AATGGCTGGCTACTATGGAG CTCTTTGCACATTGTATGGCT
Lcn2	Forward Reverse	GAAATATGCACAGGTATCCTCAG AGAAGATGATGTTGTCGTCCT
Csfr3	Forward Reverse	CCGCCAGTTTGTATCATGTC ACTGGAAGGTTTCCTCTGTC
Pf4	Forward Reverse	CACTTAAGAGCCCTAGACCC CTGGTGATGTGCTTAAGATGG
Mll1	Forward Reverse	TGAACATCCTCAACCCACTC ATACACAAACTCTACATGCCCA
Mll2	Forward Reverse	CTGCTTACCAAGAATAACCTGAG CACTCTCCATTCTGACATCCT
Mll3	Forward Reverse	CCTGCAAGATACATCAACCAC CAATGAAGTGTTGAATCGCCT
Wbp7	Forward Reverse	TATGATGGGAAGGGTATTGGG GCCTCAGTTAAGAAAGCGAC
Cdk6 promoter	Forward Reverse	AAAAGGAGCGACCCGAGAC GTATGATTCACTTGTGAGTCTGATT
Kit promoter	Forward Reverse	TAAAAGTTGCGCGTGGGTGA CAAGCAAGCCCGAGATTCGT
Etv6 promoter	Forward Reverse	GTCACAGTGGTGGTCTACCC TGCAGTGAAACAAGCGGTTC

Supplementary Table 7. shRNA sequences used in this study

target	*sequence*
Retroviral shRNA sequences (97-mer mir30 insert, in TRN and LMN vectors)	
Ren.713	TGCTGTTGACAGTGAGCGCAGGAATTATAATGCTTATCTATAGTGAAGCCACAGATGTATAGATAAGCAT TATAATTCCTATGCCTACTGCCTCGGA
Wdr5.1765	TGCTGTTGACAGTGAGCGCCTGGTATCACTCAGTAAGCTATAGTGAAGCCACAGATGTATAGCTTACTG AGTGATACCAGTTGCCTACTGCCTCGGA
Wdr5.2837	TGCTGTTGACAGTGAGCGATTGAACTCTGTTGTAGATTTATAGTGAAGCCACAGATGTATAAATCTACAA CAGAGTTCAACTGCCTACTGCCTCGGA
Mll1.13303	TGCTGTTGACAGTGAGCGCCCGCGGTATTATCCTAATTTATAGTGAAGCCACAGATGTATAAATTAGGA TAATACCGCGGTTGCCTACTGCCTCGGA
Mll2.5430	TGCTGTTGACAGTGAGCGACCGATGTAAACAAATCATGAATAGTGAAGCCACAGATGTATTCATGATTT GTTTACATCGGCTGCCTACTGCCTCGGA
Mll3.1099	TGCTGTTGACAGTGAGCGCCACCTTGGAGCCACTATCAAATAGTGAAGCCACAGATGTATTTGATAGTG GCTCCAAGGTGTTGCCTACTGCCTCGGA
Wbp7.6965	TGCTGTTGACAGTGAGCGATTCAGTCGTGTTCGCATGAAATAGTGAAGCCACAGATGTATTTCATGCGA ACACGACTGAACTGCCTACTGCCTCGGA
Lentiviral shRNA (in pLKO1-Puro vector), used for in vitro re-plating assay	
shCtrl	CGTGCATAATAAGAATCCAAA
shWdr5	GCAGCGTTAGAGAACGACAAA
Lentiviral shRNA (in pLKO1-GFP vector), used for in vivo transplantation assay	
shCtrl	CGTGCATAATAAGAATCCAAA
shWdr5-1	CGTGCATAATAAGAATCCAAA
shWdr5-2	GCCGTTCATTTCAACCGTGAT
shWdr5-3	GCCAAACTATGCCCTGAAGTT
Lentiviral shRNA (in pLV719G vector), used for knockdown of WDR5 in human cells	
shLuc	GATATGGGCTCACTGAGACTACTT
shWDR5-1	GCCAAACTATGCTCTAAAGTT
shWDR5-2	GCTCAGAGGATAACCTTGTTT

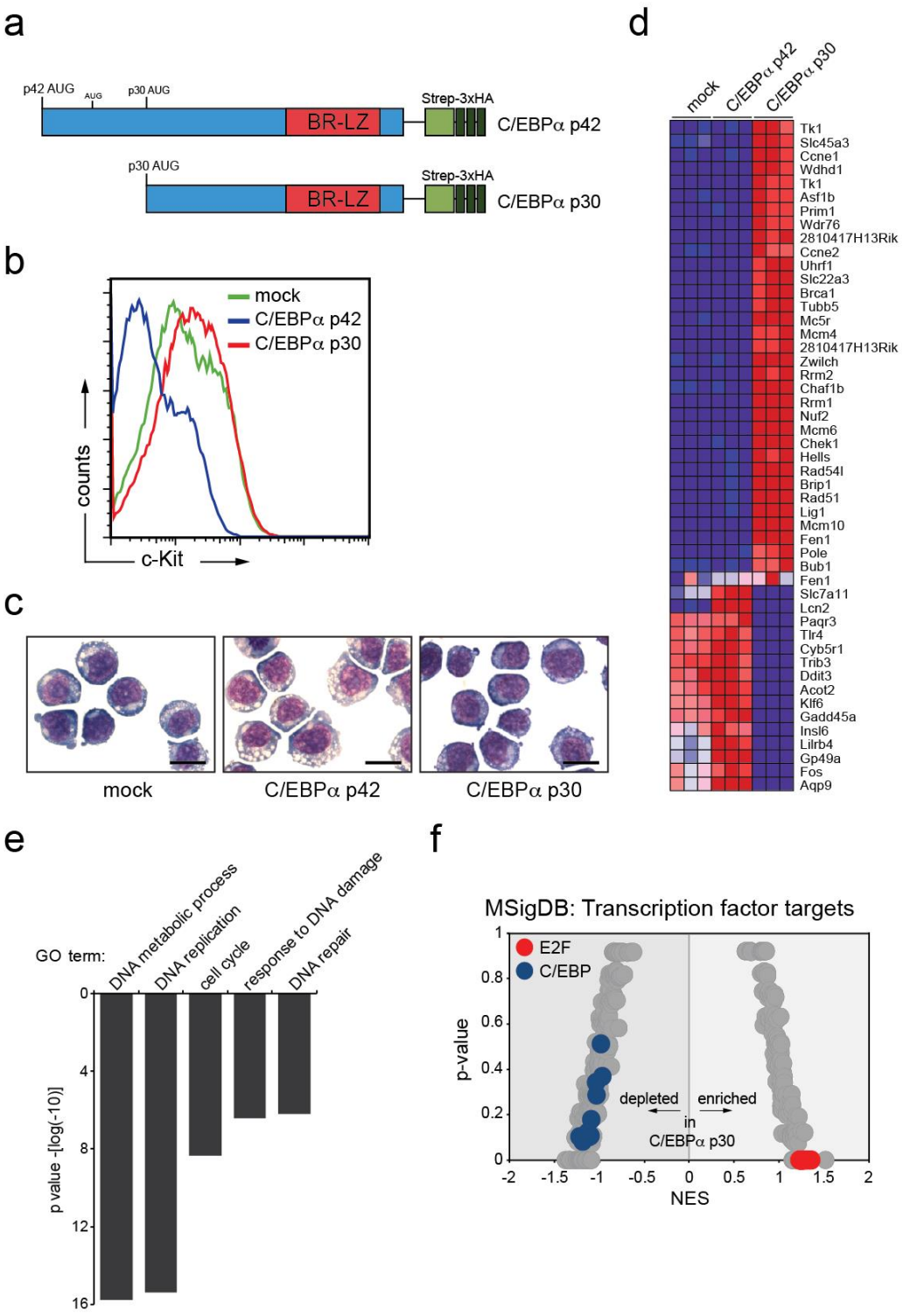

Supplementary Figure 1. An isogenic cell system to study cellular effects of C/EBPα variants. (a) Schematic representation of constructs used in this study. The Strep-3xHA tag was fused to the C-terminus of C/EBPα p42 or p30. **(b)** Flow cytometric analysis of c-Kit expression of FDCP-1 cells expressing C/EBPα p42 or

p30. **(c)** Histological staining of cytospin preparations of FDCP-1 cells expressing C/EBPα p42 or p30. Scale bar, 10 µm **(d)** Heatmap representations of the top 47 genes differentially regulated upon p30 expression in FDCP-1 cells (FDR 0.01, fold change >6) **(e)** Gene Ontology (GO)-analysis of genes shown in (e) **(f)** Gene Set enrichment (GSEA) for all transcription factor target gene sets available from the MSigDB. p-values are plotted versus normalized enrichment score (NES) for each gene set. Gene sets for E2F and C/EBP transcription factors are highlighted in red and blue, respectively.

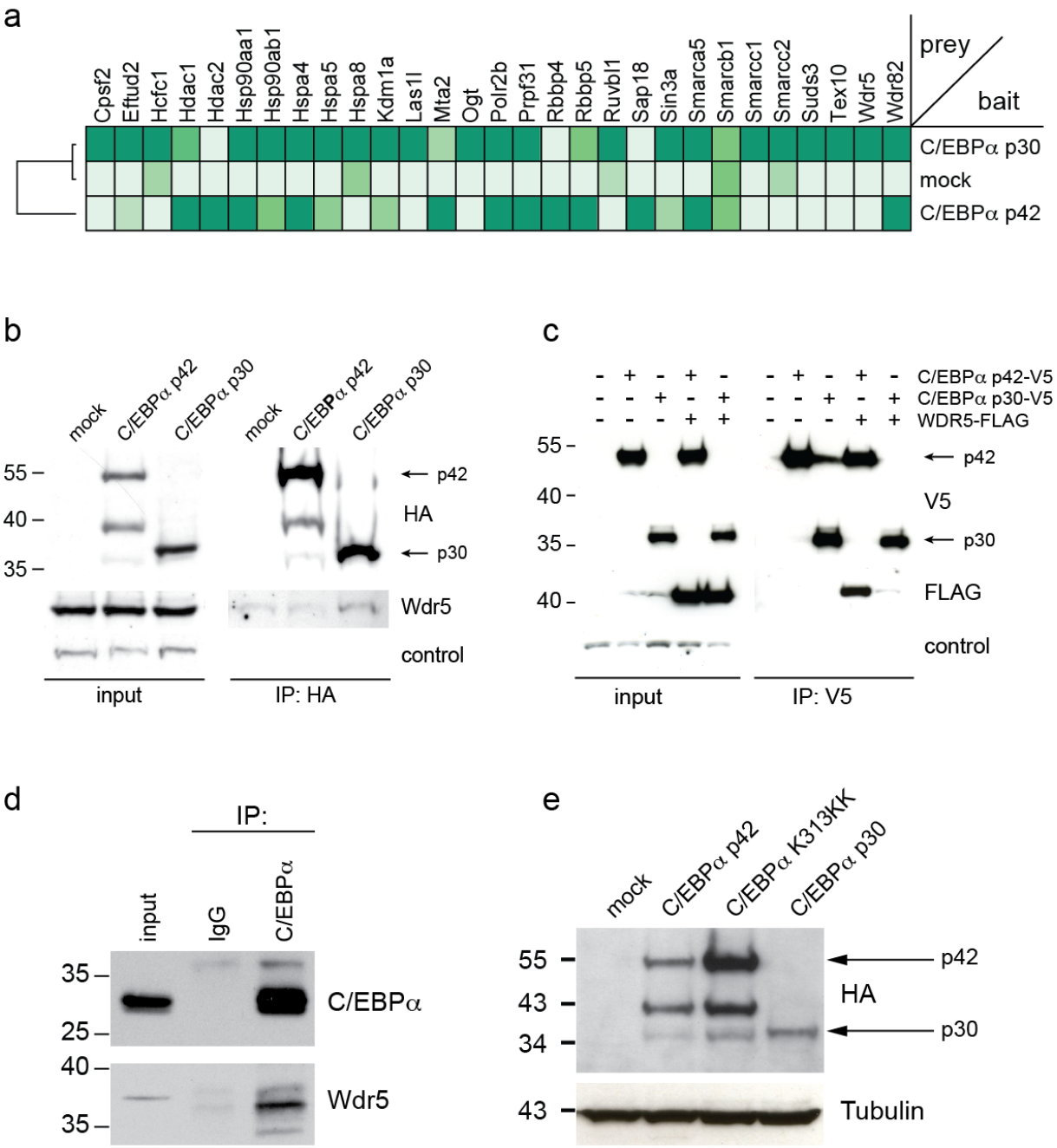

Supplementary Figure 2. Wdr5 preferably interacts with C/EBPα p30 in myeloid cells (a) Proteins present in the p42 and/or p30 AP-MS datasets were filtered for proteins that were previously found associated with Wdr5 and MLL (as published in the CORUM database, http://mips.helmholtz-muenchen.de/genre/proj/corum/). Data are presented based on average spectral counts of each protein in the respective AP-MS datasets. **(b)** Left panel: extracts from FDCP-1 cells expressing tagged variants of p42 or p30 were analyzed by Western blot for expression of HA and Wdr5. Right panel: Western blot analysis of HA and Wdr5 from anti-HA-purifications of

tagged C/EBPα variants from FDCP-1 cell lines stably expressing p42 and p30. **(c)** Left panel: extracts from HEK293 cells transfected with indicated tagged variants of p42, p30 and Wdr5 were analyzed by Western blot for expression of V5 and FLAG. Right panel: Western blot analysis of FLAG and V5 from anti-V5-immunoprecipitates of the same samples. **(d)** Western blot analysis of C/EBPα and Wdr5 from IgG- and anti-C/EBPα immunoprecipitates from lysates of *Cebpa*$^{p30/p30}$ cells. **(e)** Extracts from FDCP-1 cells expressing tagged variants of p42, p42 K313KK or p30 were analyzed by Western blot for expression of HA and tubulin. Representative images of at least 2 replicate experiments are shown. Note that tagged variants of p42 and p30 migrate at higher molecular weight than 42 and 30 kDa, respectively. The additional HA-reactive band at 40 kDa in p42-expressing samples arises from tranlation initiation at an ATG codon that lies between the initiation codons of p42 and p30 (see Supplementary Fig. 1a).

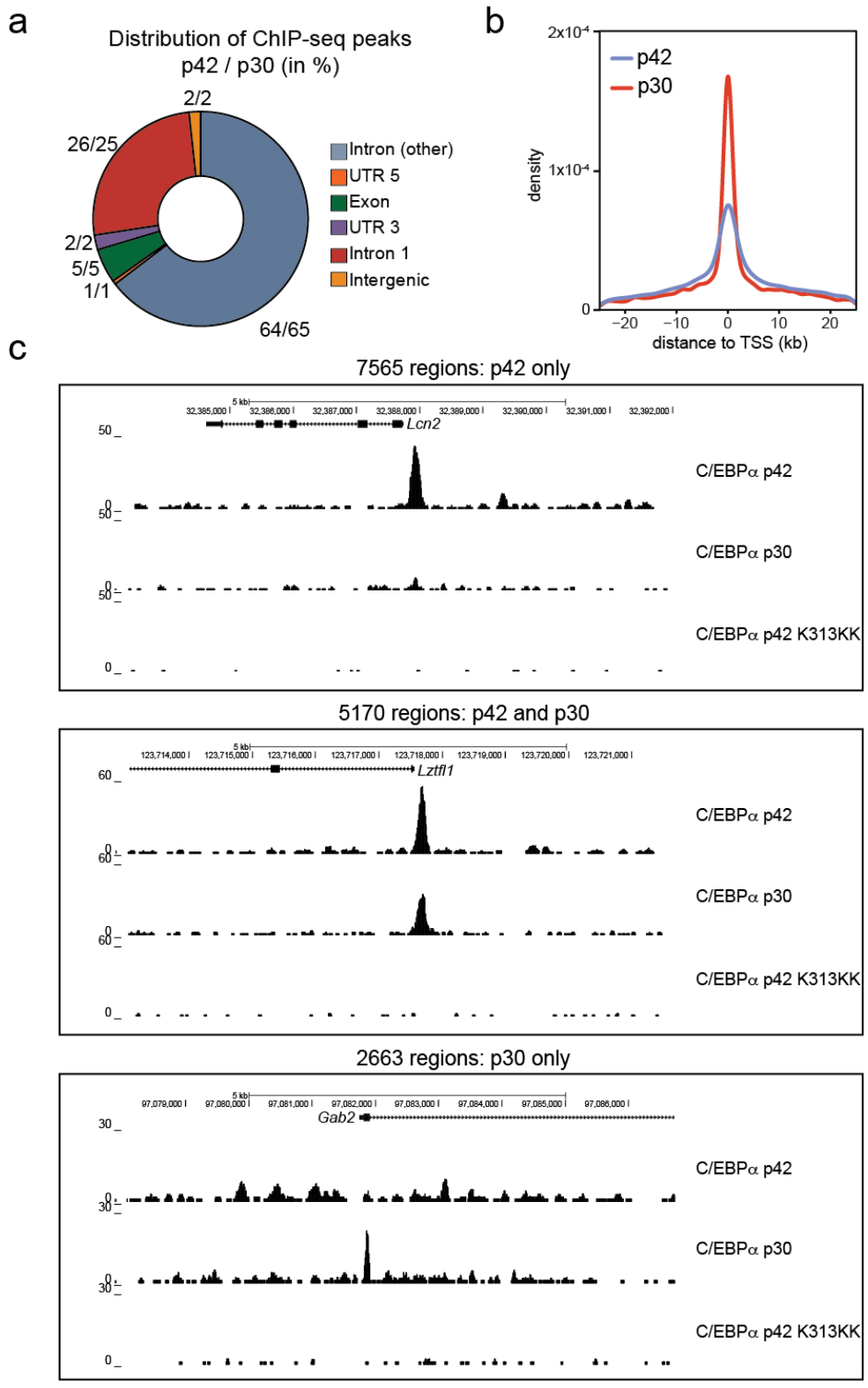

Supplementary Figure 3. C/EBPα variants display differential chromatin binding. (**a)** Distribution of p42/p30 binding sites at various genomic loci. Numbers represent percentages for p42 and p30, respectively. **(b)** Relative distances of p42-

and p30-ChIP-seq peaks to annotated Transcription Start Sites (TSS) **(c)** Representative UCSC genome browser tracks for promoters bound by C/EBPα p42 and p30 (upper panel), promoters bound by C/EBPα p42, but not p30 (middle panel), or promoters bound by C/EBPα p30, but not p42 (lower panel). The specificity of our experimental approach is validated by a control ChIP-seq experiment for a DNA-binding deficient C/EBPα mutant (K313KK), which did not show any significant chromatin association.

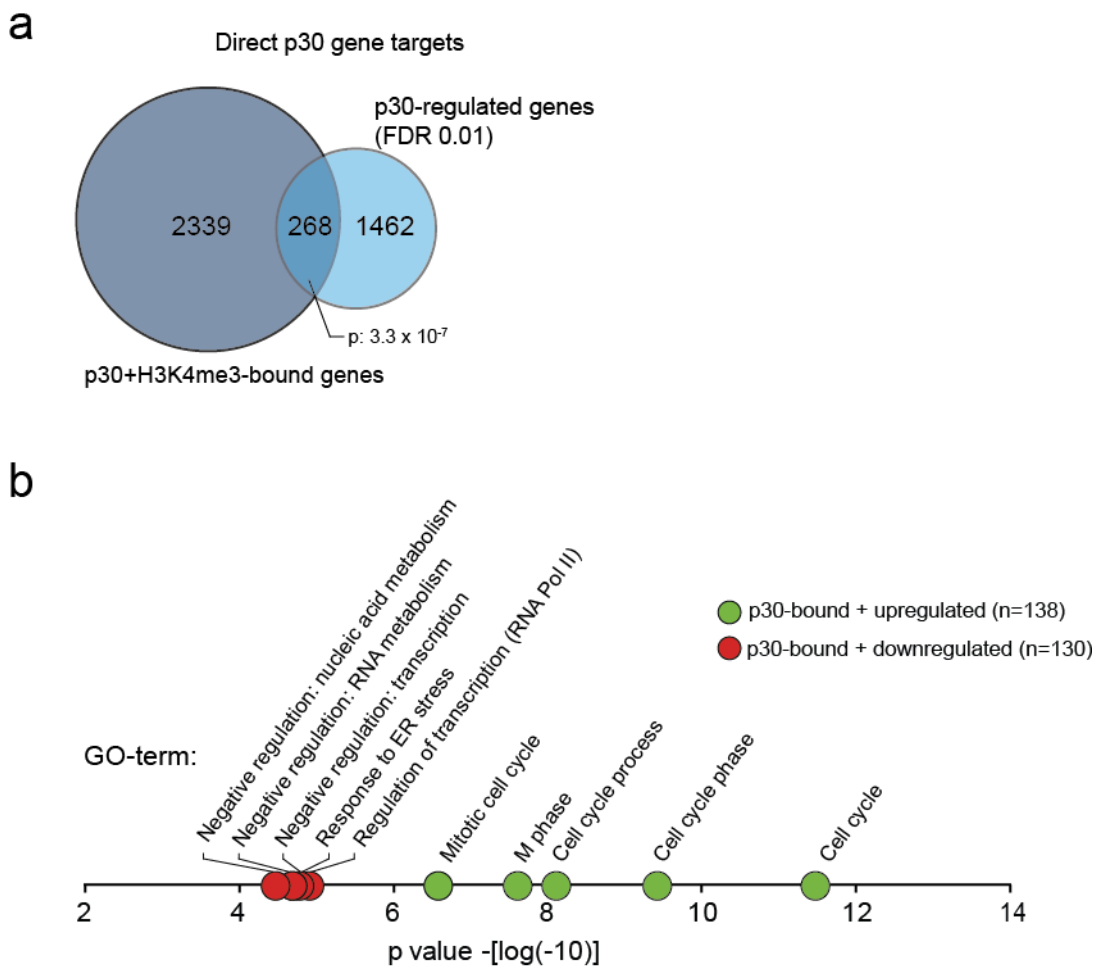

Supplementary Figure 4. C/EBPα p30 regulates the expression of distinct gene sets. (a) The Venn diagram represents an intersection of genes whose promoters were bound by p30 and were marked with H3K4me3 to indicate active transcription (left circle, dark blue, 2607 genes) and genes whose expression is de-regulated by p30 expression (right circle, light blue, 1730 genes, FDR 0.01). The 268 genes in the intersection are present in both datasets and are therefore designated “direct p30 gene targets”. **(b)** Functional annotation of direct p30 gene targets. The list of genes derived in (A) was further subdivided in up-regulated (green) and down-regulated genes (red). Functional annotation was done based on GO terms describing Biological Processes using DAVID. p-values for the top 5 biological processes are plotted for each gene set.

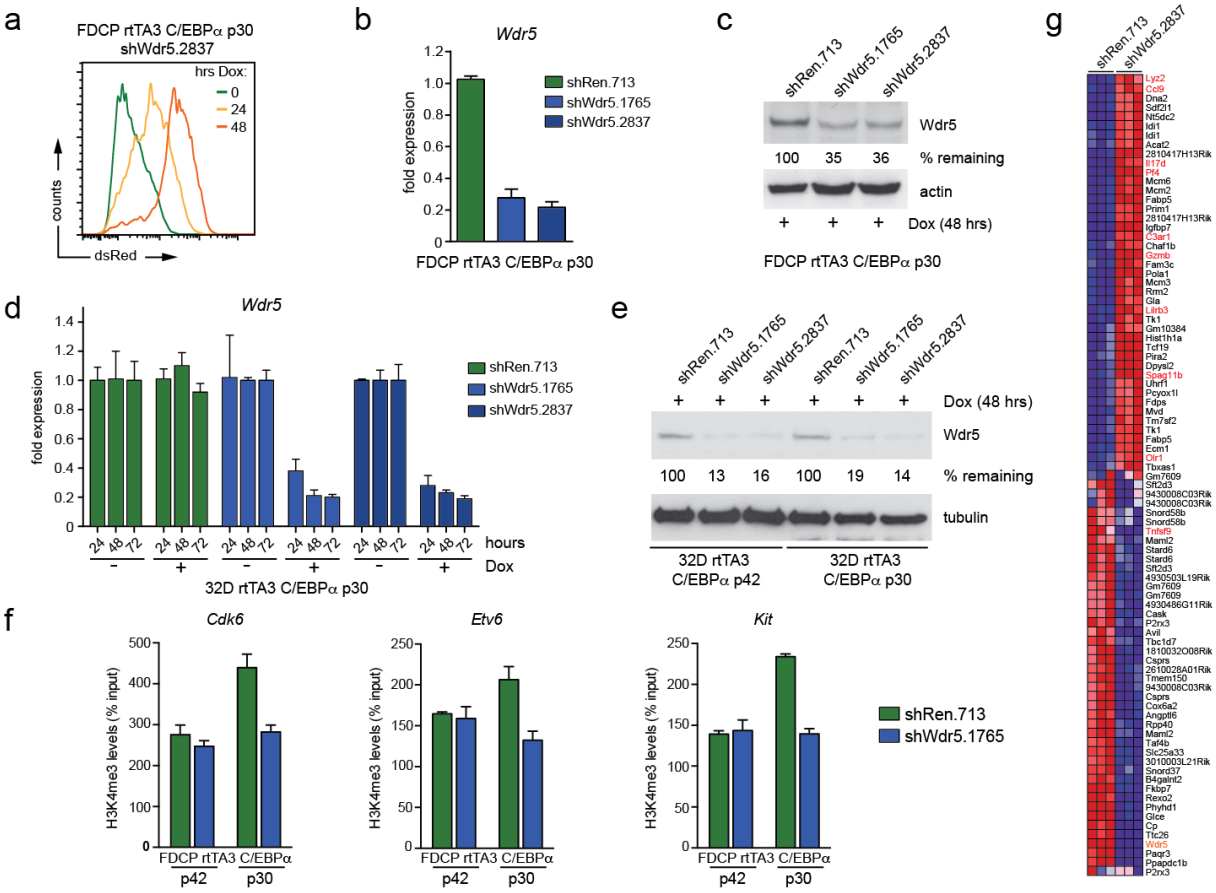

Supplementary Figure 5. Inducible shRNA-mediated knockdown of Wdr5 in p30-expressing cells reduces H3K4me3 levels on promoters of p30 target genes and induces upregulation of myeloid gene expression. (a) Flow cytometric analysis of dsRed-reporter induction in FDCP-1 rtTA3 p30 cells upon Dox administration at indicated timepoints. **(b)** qRT-PCR- and **(c)** Western Blot analysis of Wdr5 expression in FDCP-1 rtTA3 p30 cells expressing indicated shRNA constructs after 48 h of Dox treatment. Representative images of at least 2 replicate experiments are shown. **(d)** qRT-PCR- and **(e)** Western Blot analysis of Wdr5 expression in 32D rtTA3 p30 cells expressing indicated shRNA constructs after 48 hrs of Dox treatment. Representative images of at least 2 replicate experiments are shown. **(f)** qPCR analysis of the indicated cell types for specific enrichment on promoters of the *Cdk6* (left), *Etv6* (middle) and *Kit* (right) genes after H3K4me3 ChIP. **(g)** Heatmap representation of differentially regulated genes in FDCP-1 rtTA3 p30 cells expressing indicated shRNA constructs after 48 h of Dox treatment (FDR 0.05). Myeloid specific genes and are highlighted in red. Wdr5 is highlighted in orange. Data are presented as mean +/- standard deviation (SD) of triplicate experiments

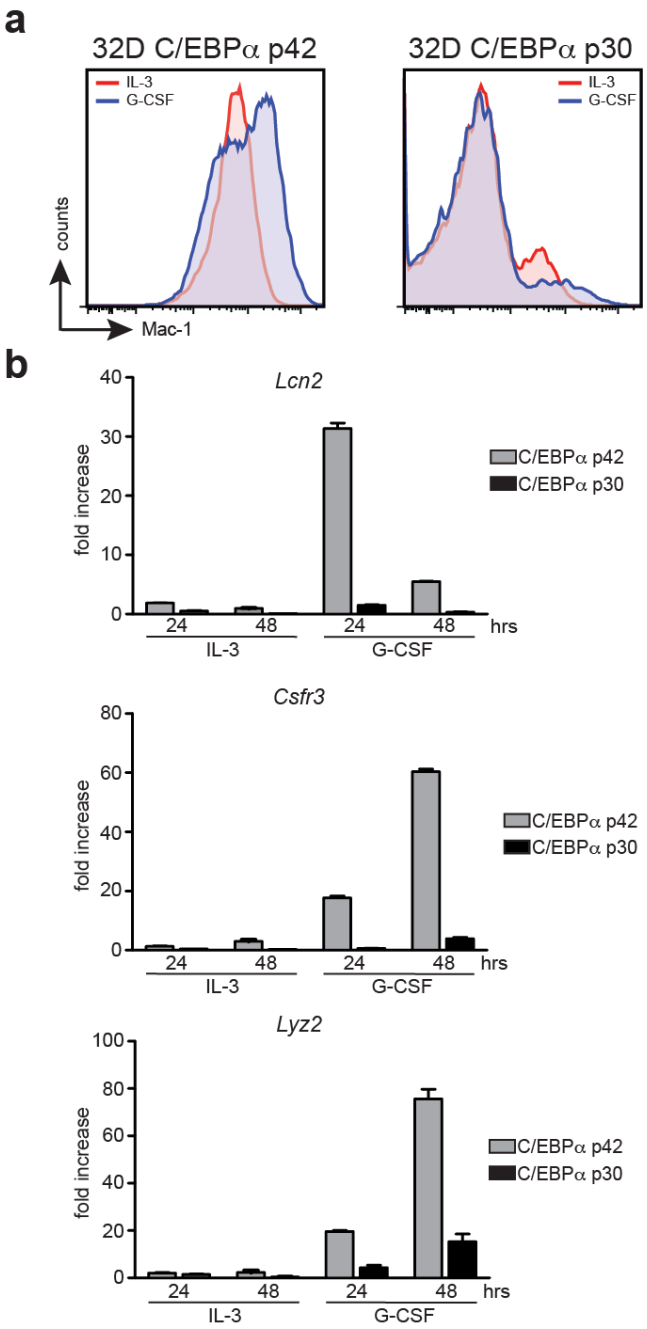

Supplementary Figure 6. Effects of C/EBPα p42 and p30 isoforms and Wdr5 on the granulocytic differentiation potential of 32D cells (a) Flow cytometric analysis of Mac-1 surface expression in 32D cells expressing C/EBPα p42 (left panel) or C/EBPα p30 (right panel) after culture in the presence of IL-3 (5 ng/mL, red curves) or G-CSF (10 ng/mL, blue curves) **(a)** qRT-PCR-analysis of the indicated genes in 32D cell expressing C/EBPα p42 (white bars) or C/EBPα p30 (black bars) after culture in the presence of IL-3 or G-CSF for the indicated time. Data are presented as mean +/- standard deviation (SD) of triplicate experiments

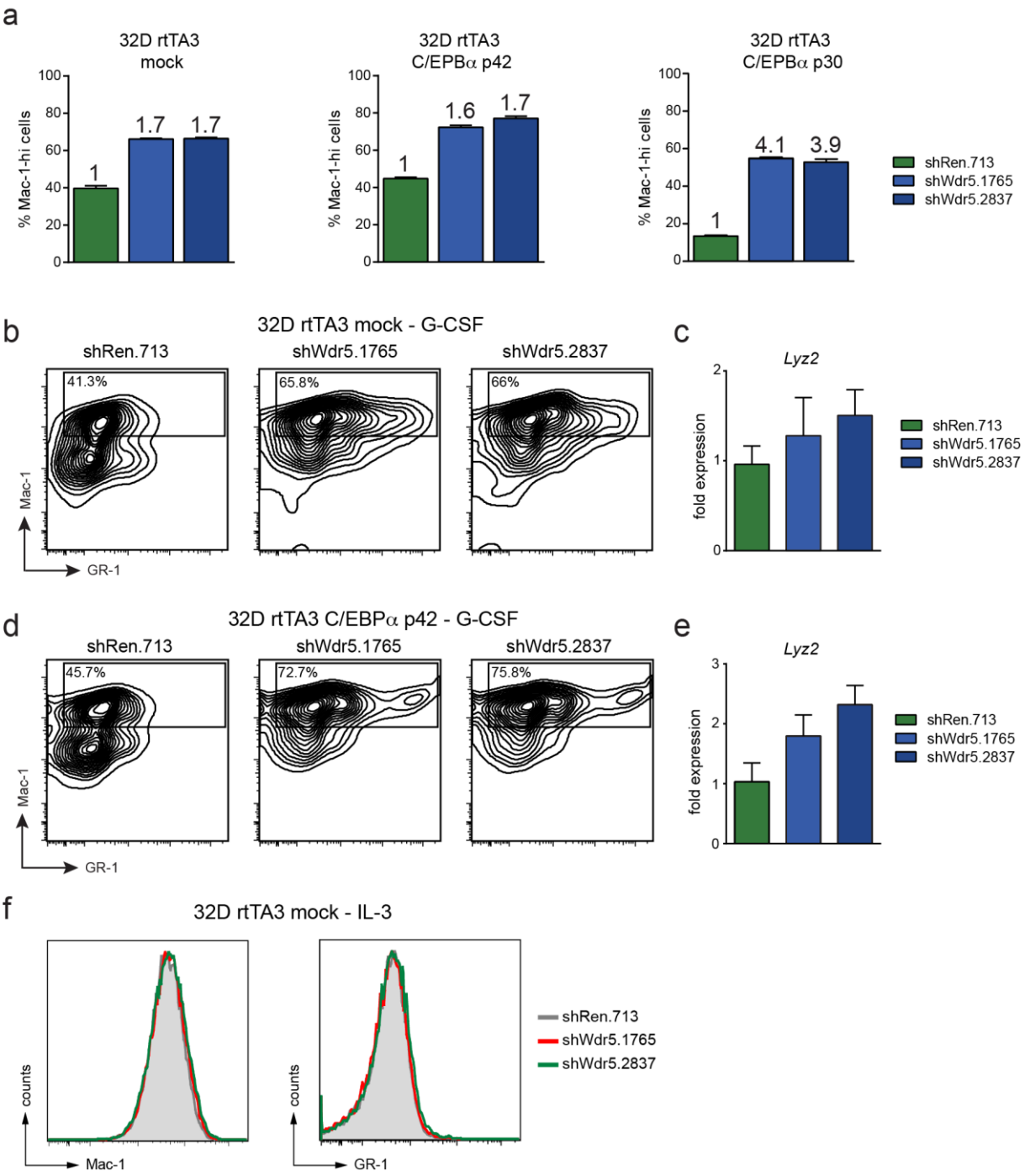

Supplementary Figure 7. Knockdown of Wdr5 has marginal effects on the granulocytic differentiation potential of 32D cells (a) statistical representation of percentages of Mac-1^{hi} cells from the G-CSF experiment described in Fig. 2c and Supplementary Fig. 7b-e. Numbers above bars represent the fold induction in Mac-1^{hi} cells over cells expressing a control shRNA- **(b)** Flow cytometry analysis for Mac-1 and GR-1 surface markers of 32D rtTA3 cells expressing indicated shRNA constructs 96 h after Dox treatment and 48 h after exposure to G-CSF (10 ng/mL). Presented

events are gated on the dsRed+ population. **(c)** qRT-PCR analysis of *Lyz2* expression in 32D rtTA3 cells transduced with indicated shRNA constructs after 96 h of Dox treatment followed by 48 h exposure to G-CSF (10 ng/mL). Data are presented as mean +/- standard deviation (SD) of triplicate experiments. **(d)** Flow cytometry analysis for Mac-1 and GR-1 surface markers of 32D rtTA3 p42 cells expressing indicated shRNA constructs 96 h after Dox treatment and 48 h after exposure to G-CSF (10 ng/mL). Presented events are gated on the GFP+ dsRed+ population. **(e)** qRT-PCR analysis of *Lyz2* expression in 32D rtTA3 p42 cells transduced with indicated shRNA constructs after 96 h of Dox treatment followed by 48 h exposure to G-CSF. Data are presented as mean +/- standard deviation (SD) of triplicate experiments. (f) Flow cytometry analysis for Mac-1 and GR-1 surface markers of 32D rtTA3 cells expressing indicated shRNA constructs 96 h after Dox in the presence of IL-3 (5 ng/mL).

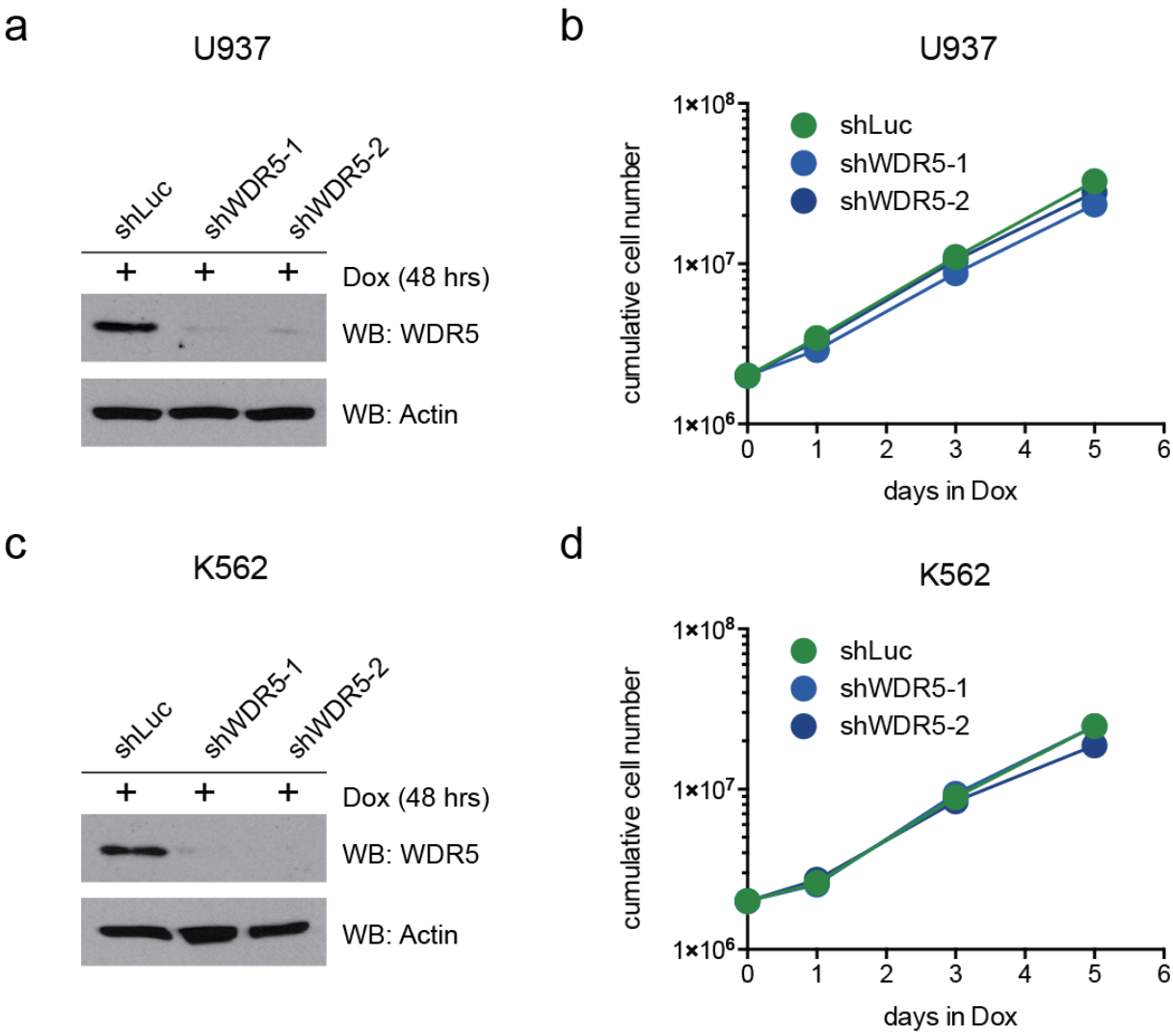

Supplementary Figure 8. Knockdown of WDR5 does not impair proliferation of U937 and K562 cells. (a) Extracts from U937 cells expressing indicated shRNA constructs were analyzed by Western blot for expression of WDR5 and Actin. **(b)** Proliferation curves of U937 cells expressing indicated shRNA constructs after Dox treatment. **(c)** Extracts from K562 cells expressing indicated shRNA constructs were analyzed by Western blot for expression of WDR5 and Actin. **(d)** Proliferation curves of K562 cells expressing indicated shRNA constructs after Dox treatment. Data are presented as mean +/- standard deviation (SD) of triplicate experiments. Representative images of at least 2 replicate experiments are shown.

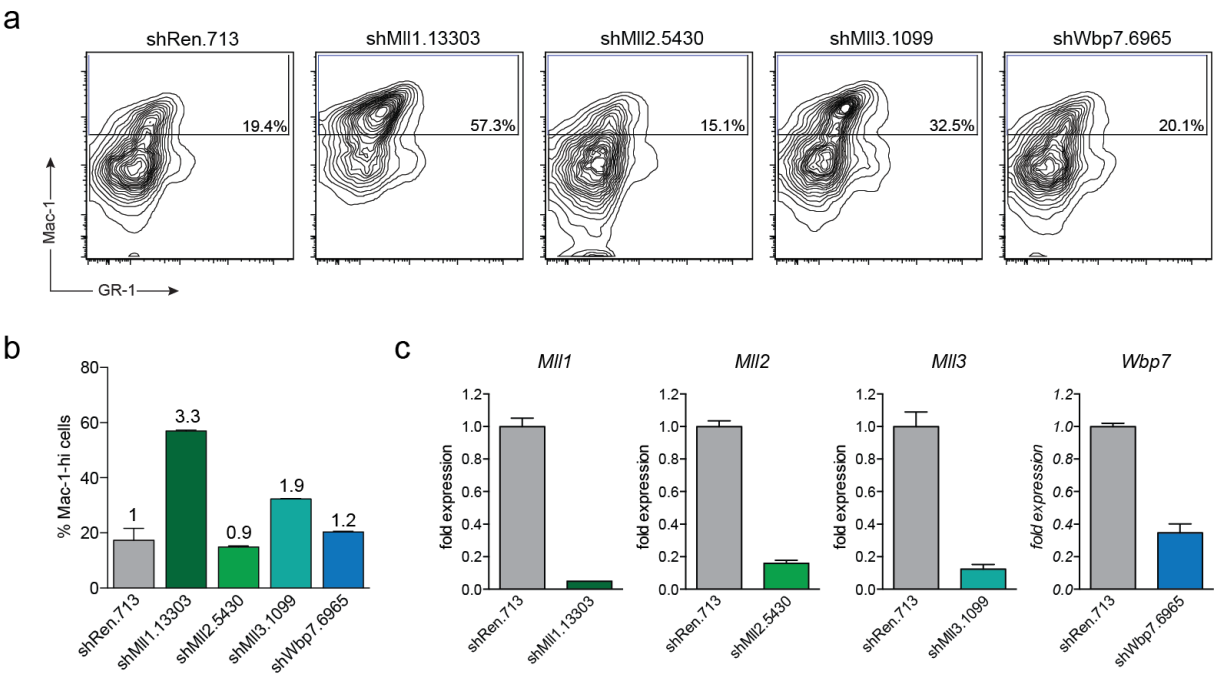

Supplementary Figure 9. Loss of Mll1 or Mll3, but not Mll2 or Mll4/Wbp7 restores granulocytic differentiation potential in C/EBPα p30-expressing cells. **(a)** Flow cytometry analysis for Mac-1 and GR-1 surface markers of 32D rtTA3 p30 cells expressing indicated shRNA constructs 96 h after Dox treatment and 48 h after exposure to G-CSF (10 ng/mL). Presented events are gated on the GFP^+ $dsRed^+$ population. **(b)** Statistical representation of percentages of Mac-1^{hi} cells from the experiment described in (a) **(c)** qRT-PCR analysis of the indicated genes *in* 32D rtTA3 p30 cells expressing indicated shRNA constructs after 48 h of Dox treatment. Data are presented as mean +/- standard deviation (SD) of triplicate experiments.

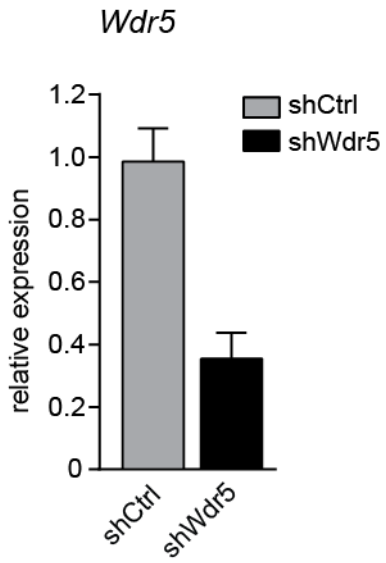

Supplementary Figure 10. Wdr5 knockdown in primary fetal liver cells from *Cebpa*$^{p30/p30}$ *mice*. qRT-PCR-analysis of Wdr5 expression levels in *Cebpa*^{p30p30} primary fetal liver cells expressing a control (grey bars) or Wdr5-targeting lentiviral shRNA construct used in Fig. 3a, b. Data are presented as mean +/- standard deviation (SD) of triplicate experiments.

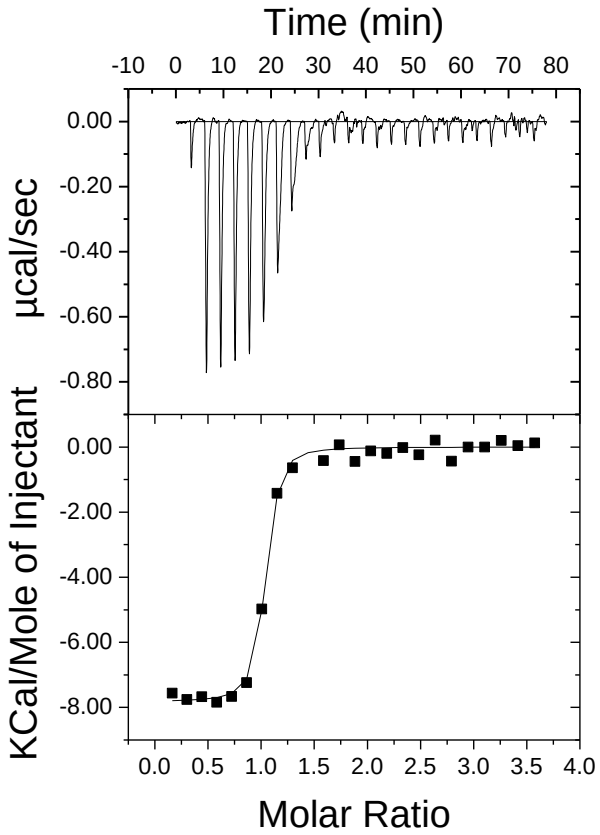

Supplementary Figure 11. OICR-9429 binds to WDR5. Binding of OICR-9429 to WDR5 was assessed by ITC. 10 µL aliquots of 300 µM compound solution were titrated over a 15 µM solution of WDR5. DMSO concentration was kept constant at 3% throughout the experiment. The titrations were performed at 25 ^{o}C in 100 mM Hepes, 150 mM NaCl, pH 7.4 using a General Electric VP MicroCal calorimeter. A K_D value of 93 ± 28 nM was calculated from 5 independent experiments.

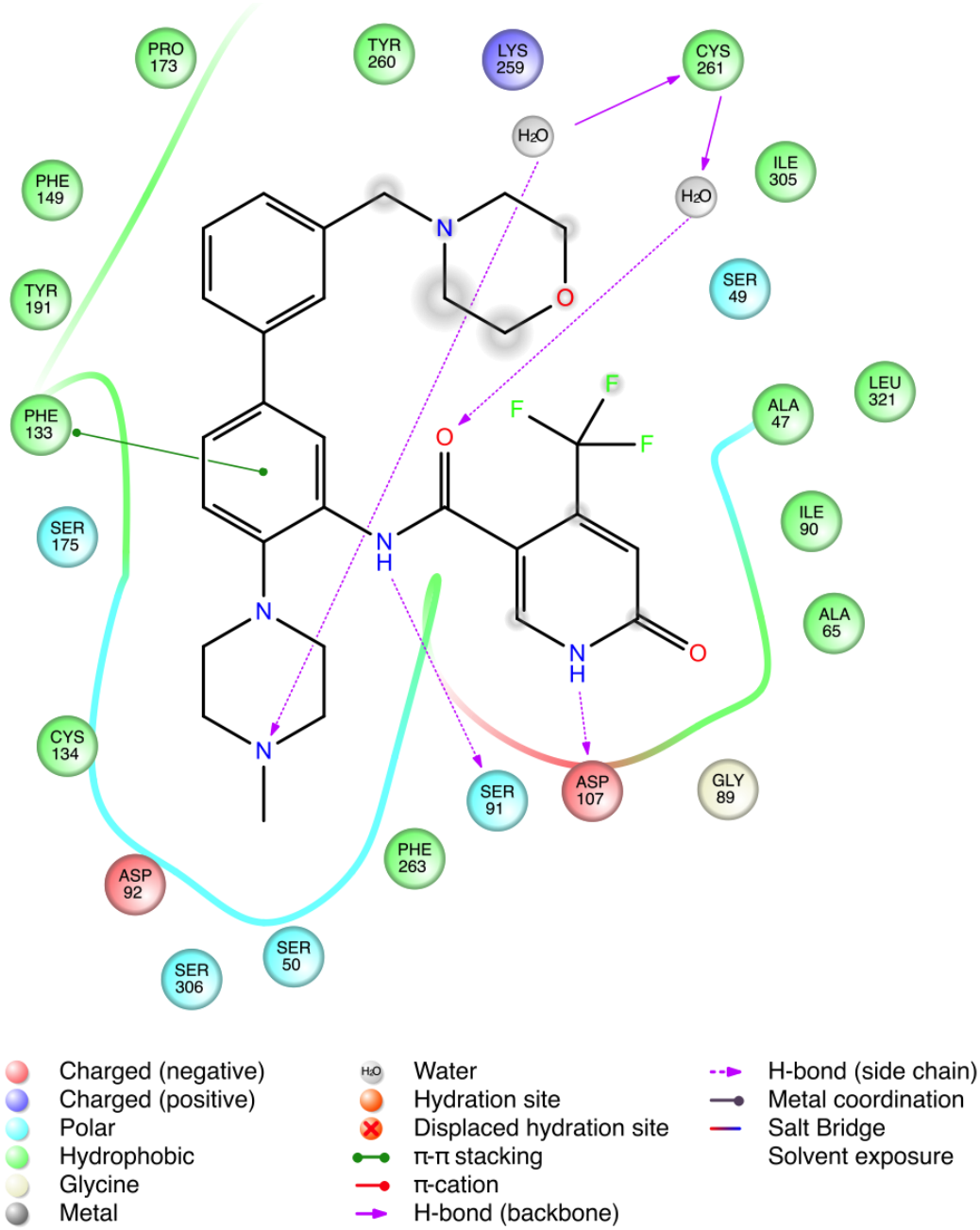

Supplementary Figure 12. Schematic illustration of key atomic interactions between OICR-9429 and WDR5. OICR-9429's south-end (methyl-piperazine), east-end (pyridinone) and amide linker form hydrogen bonds with surrounding residues of WDR5 (colored circles), while the north moiety is surrounded with hydrophobic side-chains (interaction map was generated with Maestro).

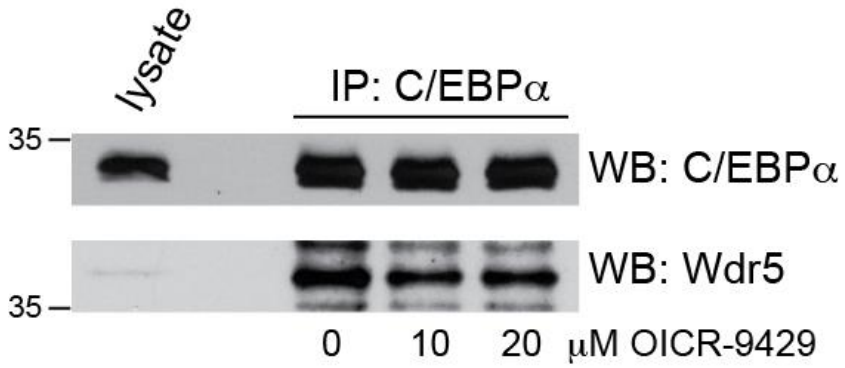

Supplementary Figure 13. OICR-9429 does not inhibit the C/EBPα p30-Wdr5 interaction. Western blot analysis of C/EBPα-immunoprecipitates from *Cepba*$^{p30/p30}$ cells treated with the indicated concentrations of OICR-9429. Representative images of at least 2 replicate experiments are shown.

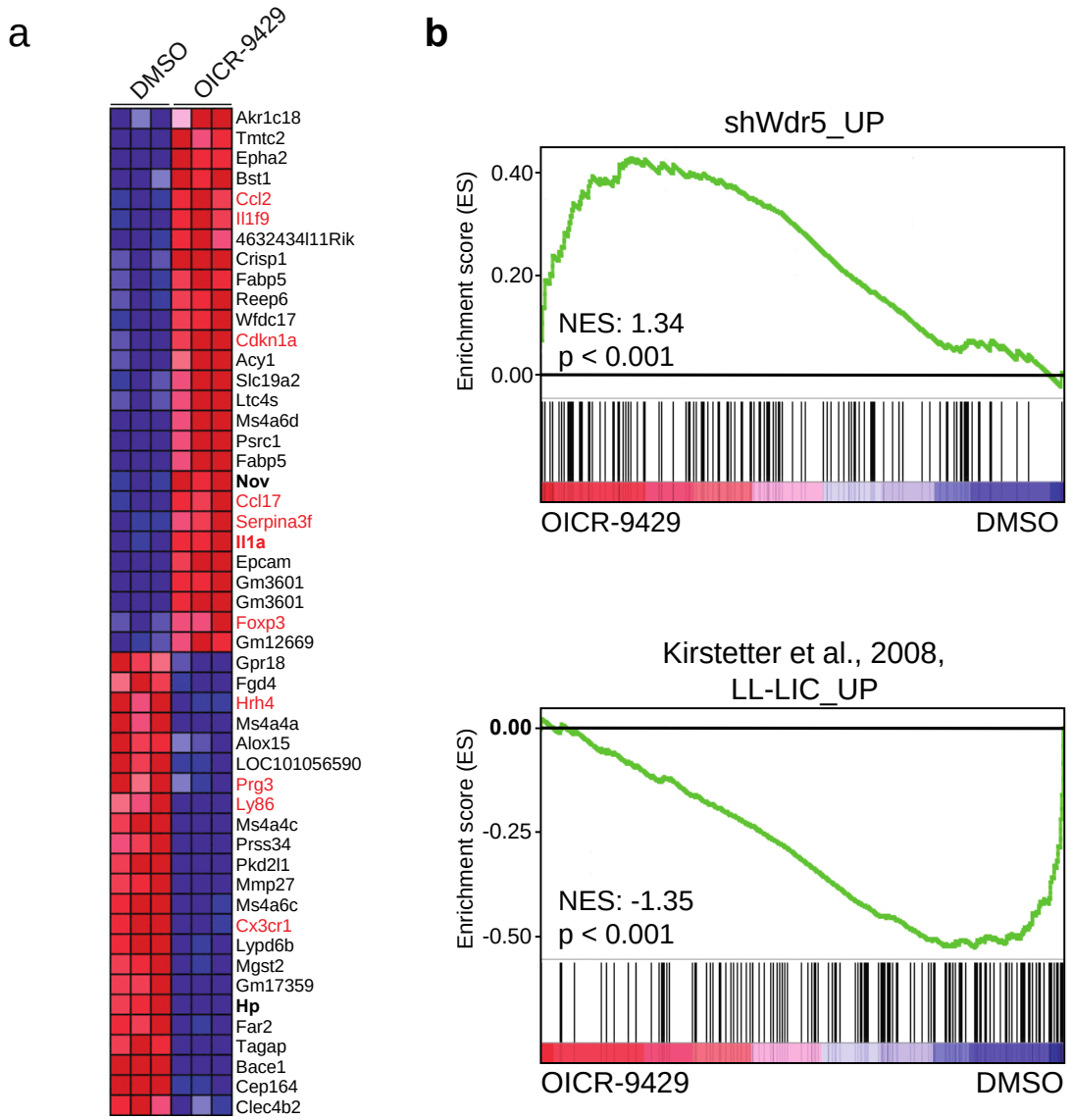

Supplementary Figure 14. Gene expression analysis of *Cebpa*$^{p30/p30}$ cells upon OICR-9429 treatment. (a) Heatmap representation of differentially regulated genes in *Cebpa*$^{p30/p30}$ cells after 72 h of OICR-9429 treatment (20 µM, FDR 0.01, fold change 1.75). Myeloid specific genes and are highlighted in red. **(b)** Gene Set Enrichment Analysis showing global up-regulation of Genes indiced by Wdr5 knockdown (top) and global down-regulation of the *Cepba*$^{p30/p30}$ LIC signature upon OICR-9429 treatment of *Cebpa*$^{p30/p30}$ cells (bottom), NES, Normalized Enrichment Score.

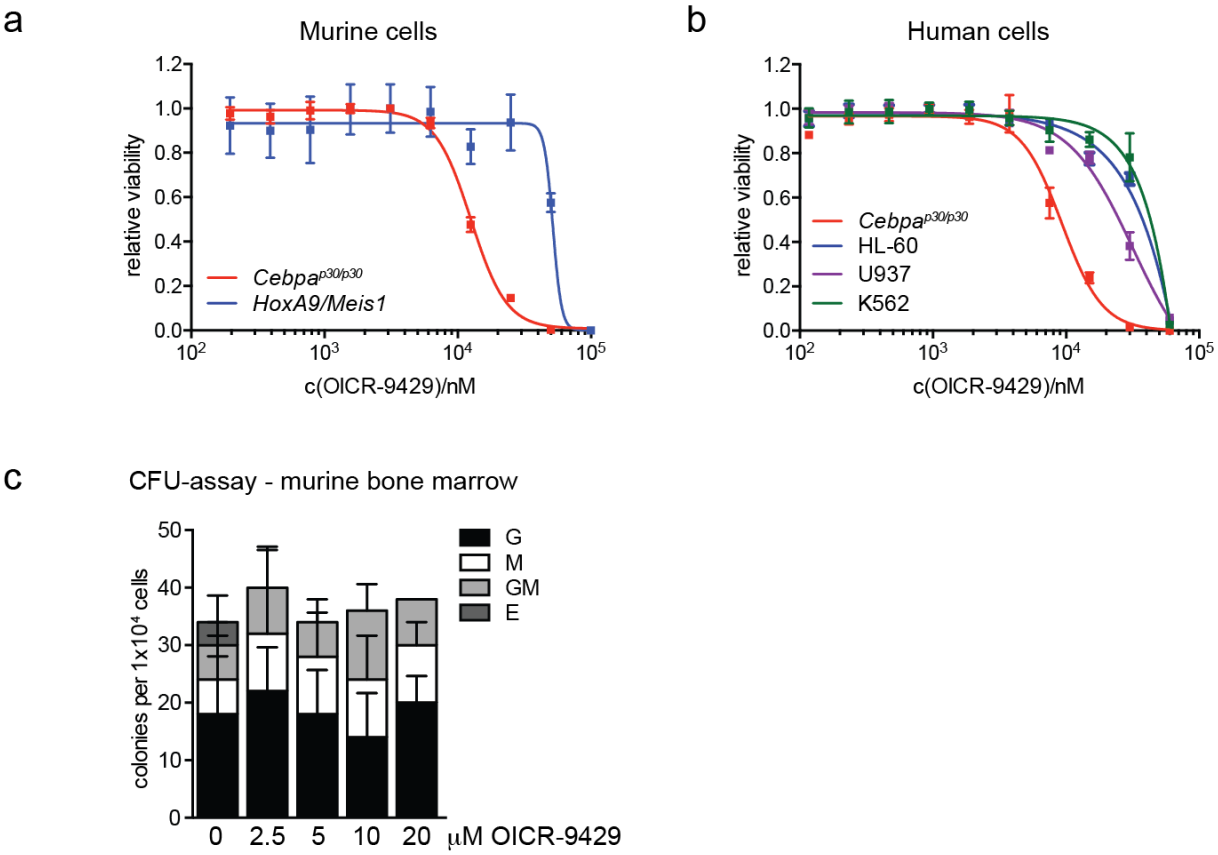

Supplementary Figure 15. *Cebpa*$^{p30/p30}$-cells are specifically sensitive to Wdr5 antagonism. (a) Dose response curves for OICR-9429 in *Cebpa*$^{p30/p30}$ cells (red) and HoxA9/Meis1-transformed wild-type cells (blue). **(b)** Dose response curves for OICR-9429 in *Cebpa*$^{p30/p30}$ cells (red), HL-60 (blue), U937 (purple) and K562 cells (green). **(c)** CFU-assay of primary murine bone marrow cells in the presence of indicated concentrations of OICR-9429. Data are presented as mean +/- standard deviation (SD) of triplicate experiments.

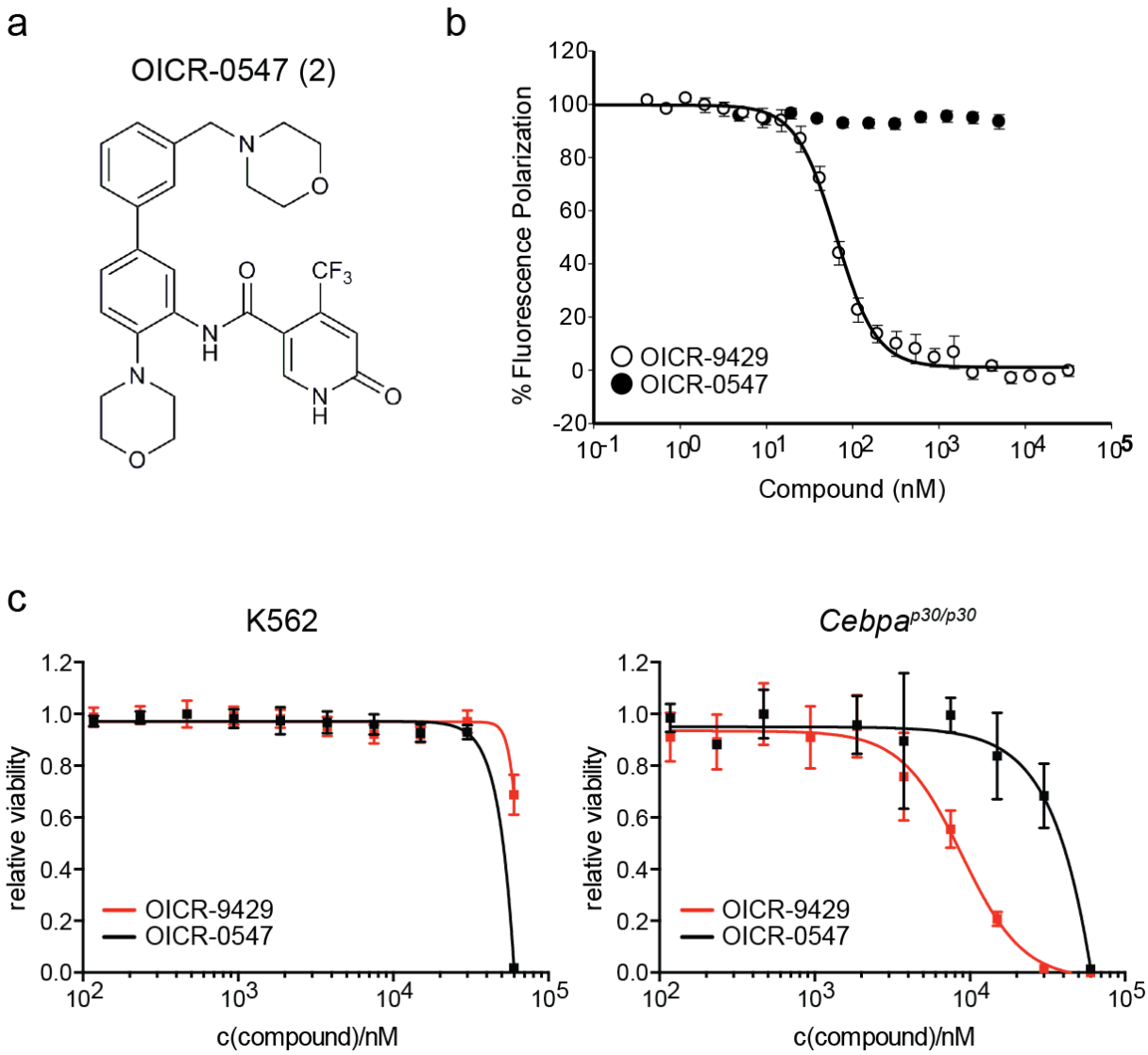

Supplementary Figure 16. OICR-0547, an inactive control compound, does not bind to WDR5 and has no effect on cellular viability. (a) Chemical structure of OICR-0547. OICR-0547 was designed as an inactive control compound where the methylpiperazine moiety was replaced with a morpholine ring, which should lead to the inability of the compound to bind in the arginine-binding pocket of WDR5. **(b)** Peptide displacement assay monitoring the decrease in fluorescence polarization (FP) signal of a modified fluorescein labeled MLL peptide upon compound-induced dissociation from WDR5. **(c)** Dose response curves for OICR-9429 (red) and OICR-0547 (black) in K562 cells (left panel) and *Cebpa*$^{p30/p30}$ cells (right panel). Note that OICR-0547 induces non-selective toxicity at high doses in both cell types, which might results from off-target activity. Data are presented as mean +/- standard deviation (SD) of triplicate experiments.

Full, uncut gel images for Figures 1, 5 and Supplementary Figures 2, 5, 8 and 13.

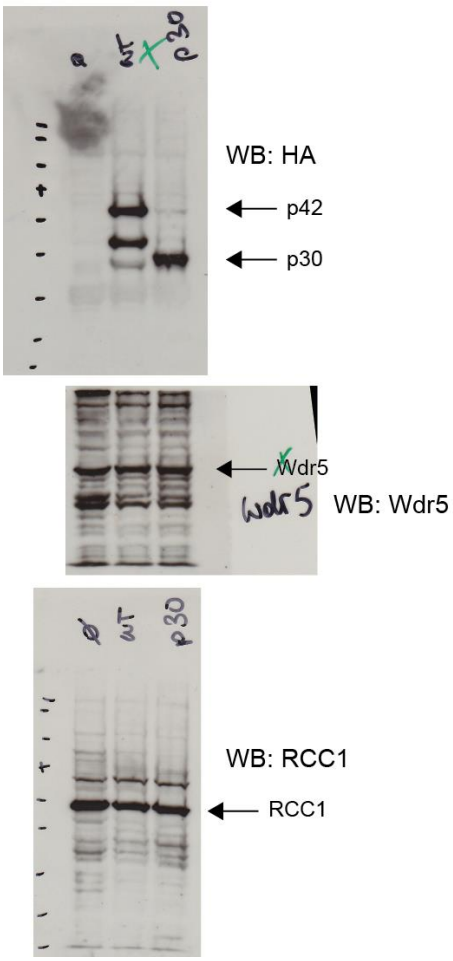

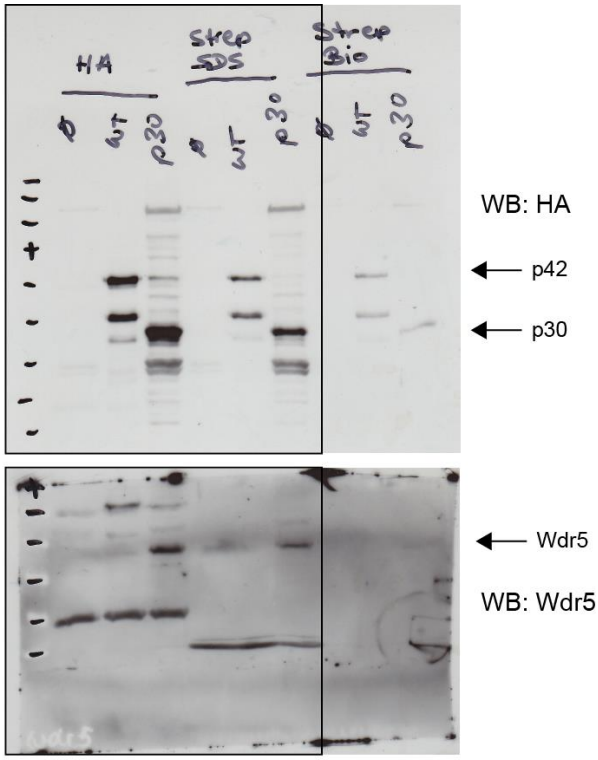

Original Gels - Figure 1b

Figure 5a

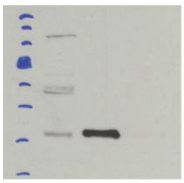

Figure 5c

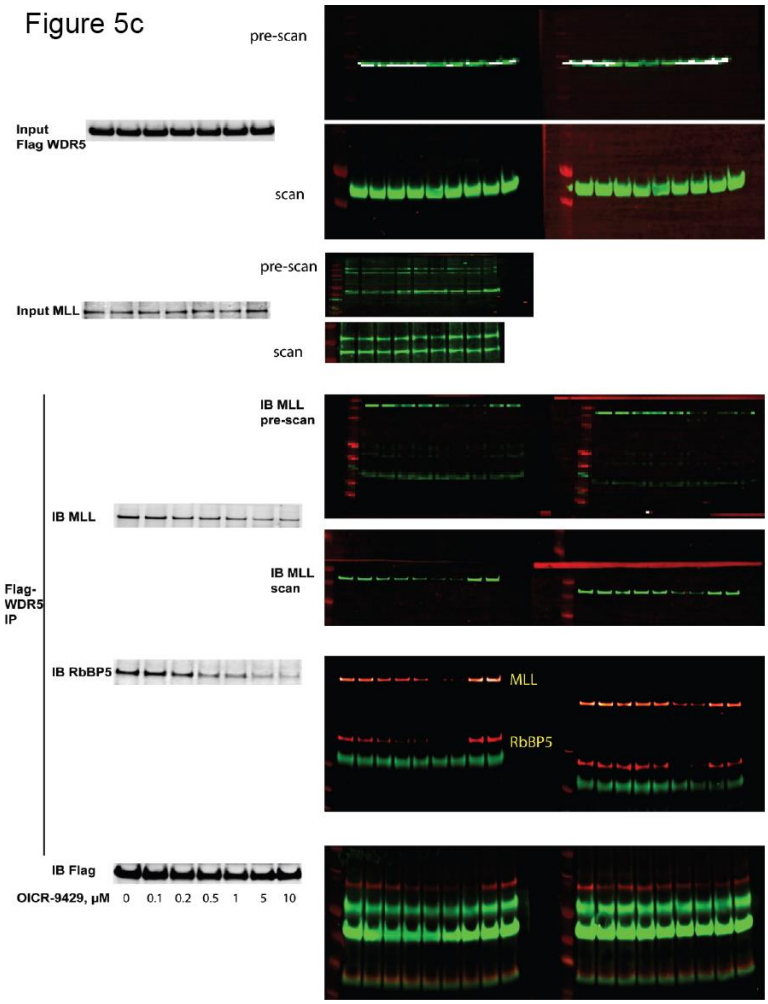

Original Gels - Figure 5

Supplementary Figure 2b

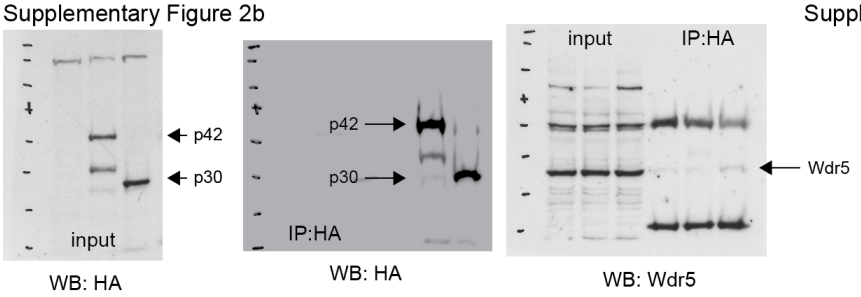

Supplementary Figure 2c

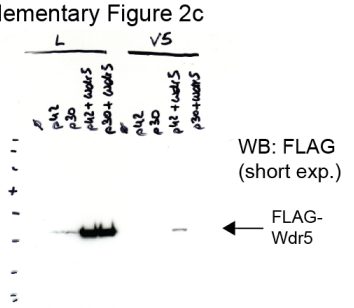

Supplementary Figure 2d

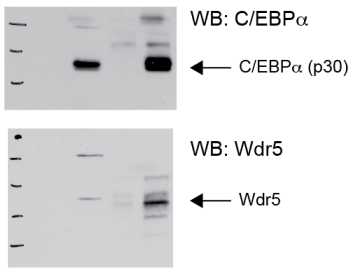

Supplementary Figure 2e

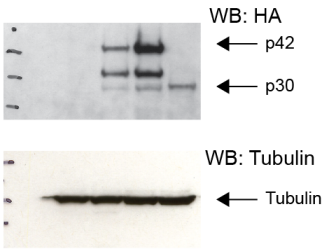

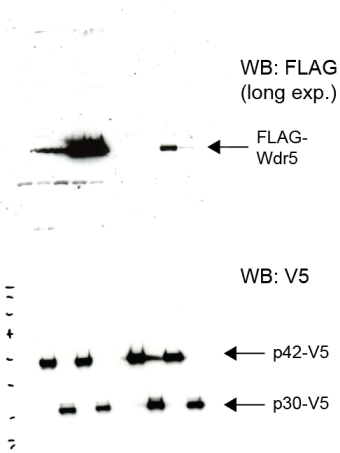

Original Gels - Supplementary Figure 2

Supplementary Figure 5c

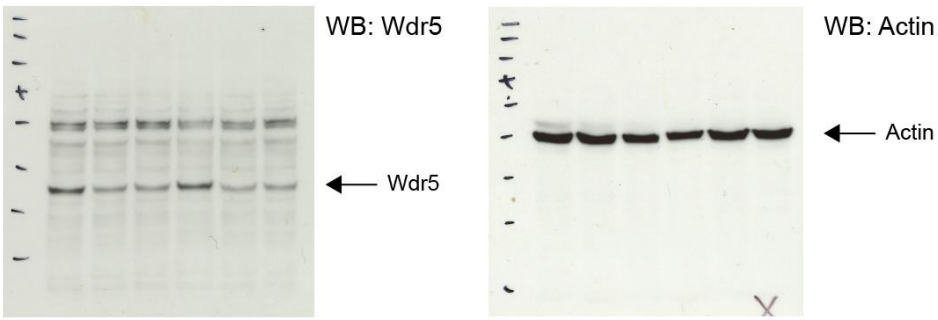

Supplementary Figure 5e

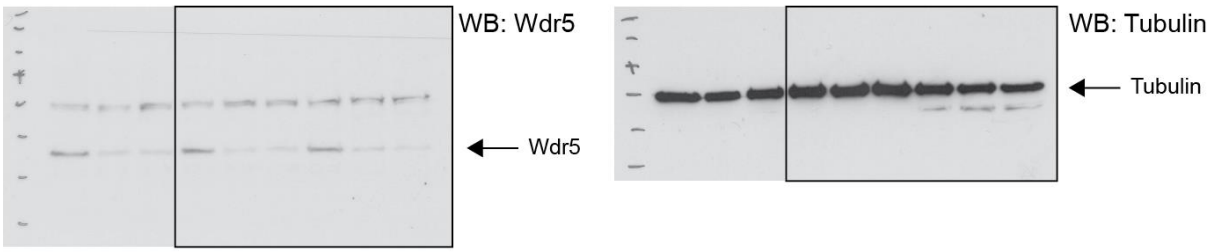

Original Gels - Supplementary Figure 5

Supplementary Figure 8a

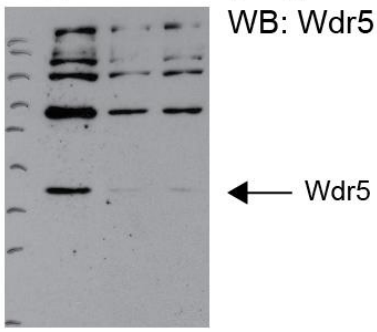

Supplementary Figure 8a+c

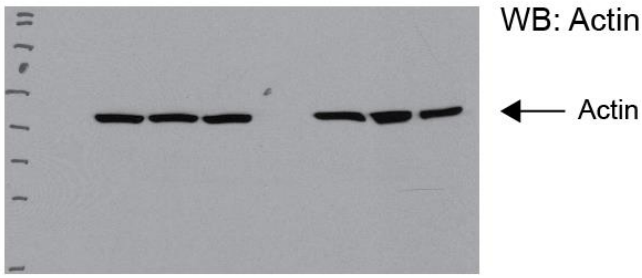

Supplementary Figure 8c

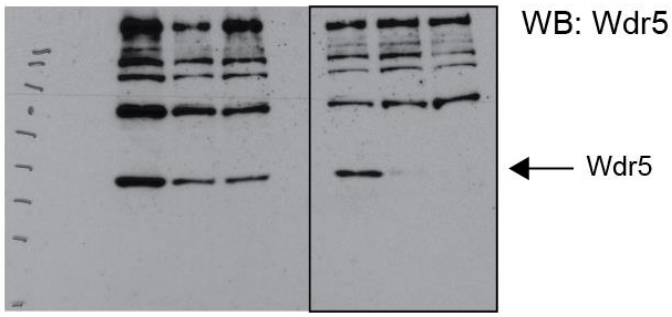

Original Gels - Supplementary Figure 8

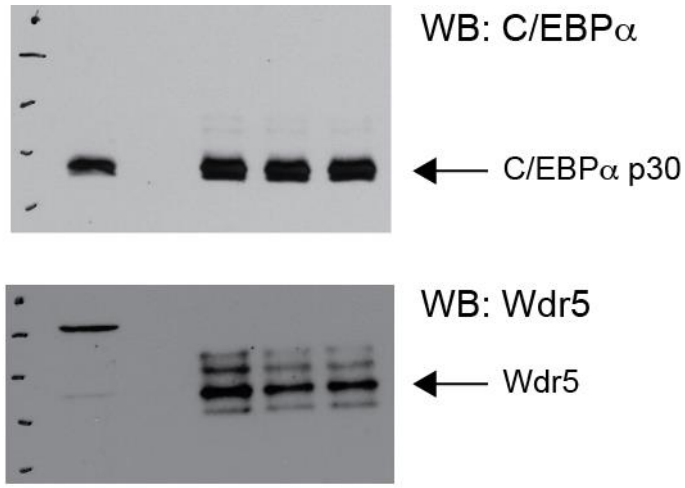

Original Gels - Supplementary Figure 13

Supplementary note to the paper

Pharmacological targeting of the Wdr5-MLL interaction in C/EBPα N-terminal leukemia

Florian Grebien[1,2*§], Masoud Vedadi[3,4*], Matthäus Getlik[5*], Roberto Giambruno[1], Amit Grover[6], Roberto Avellino[7], Anna Skucha[1], Sarah Vittori[1], Ekaterina Kuznetsova[3], David Smil[3], Dalia Barsyte-Lovejoy[3], Fengling Li[3], Gennadiy Poda[5,8], Matthieu Schapira[3,4], Hong Wu[3], Aiping Dong[3], Guillermo Senisterra[3], Alexey Stukalov[1], Kilian V. M. Huber[1], Andreas Schönegger[1], Martin Bilban[9], Christoph Bock[1], Peter J. Brown[3], Johannes Zuber[10], Keiryn L. Bennett[1], Rima Al-awar[4,5], Ruud Delwel[7], Claus Nerlov[6], Cheryl H. Arrowsmith[3,11*§] and Giulio Superti-Furga[1*§]

[1] CeMM Research Center for Molecular Medicine of the Austrian Academy of Sciences, Vienna 1090, Austria

[2] Ludwig Boltzmann Institute for Cancer Research, Vienna 1090, Austria

[3] Structural Genomics Consortium, University of Toronto, Toronto, ON, M5G 1L7, Canada

[4] Department of Pharmacology and Toxicology, University of Toronto, Toronto, ON, M5S 1A8, Canada

[5] Drug Discovery Program, Ontario Institute for Cancer Research, Toronto, ON, M5G 0A3, Canada

[6] MRC Molecular Hematology Unit, Weatherall Institute of Molecular Medicine, Oxford OX3 9DS, United Kingdom

[7] Department of Hematology, Erasmus University Medical Center, Rotterdam 3015 GE, The Netherlands

[8] Leslie Dan Faculty of Pharmacy, University of Toronto, Toronto, ON, M5S 3M2, Canada

[9] Clinical Institute of Medical and Chemical Laboratory Diagnostics, Medical University Vienna, Vienna 1090, Austria

[10] Research Institute of Molecular Pathology (IMP), Vienna 1030, Austria

[11] Princess Margaret Cancer Centre and Department of Medical Biophysics, University of Toronto, Toronto, ON, M5G 2M9, Canada

* equal contribution

[§] correspondence to

Giulio Superti-Furga: gsuperti@cemm.oeaw.ac.at, phone: +43-1-40160-70001

Cheryl H Arrowsmith: carrow@uhnresearch.ca, phone: +1-416-946-0881

Florian Grebien: florian.grebien@lbicr.lbg.ac.at, phone: +43-1-40160-71240

Chemical Synthesis - General Information

All oxygen and/or moisture sensitive reactions were carried out under N_2 atmosphere in glassware purged with N_2 prior to use. Concentrations under reduced pressure were performed by rotary evaporation at 40 °C at the appropriate pressure, unless otherwise noted. All reagents and laboratory grade solvents were purchased from commercial vendors and used as received, without further purification. The yields given refer to chromatographically purified and spectroscopically pure compounds, unless stated otherwise. **Nuclear magnetic resonance (NMR)**: 1H, 13C{1H}, DEPTq, COSY, HSQC and HMBC NMR spectra were recorded on a Bruker Avance-III 500 MHz spectrometer (500 MHz ^{1}H, 125 MHz ^{13}C). All ^{1}H NMR spectra were referenced relative to $SiMe_4$ through a resonance of the employed deuterated solvent or proteo impurity of the solvent; chloroform (7.26 ppm), acetone (2.05 ppm), DMSO (3.33 ppm) and methanol (3.31 ppm) for ^{1}H NMR; chloroform (77.00 ppm), acetone (29.84 ppm), DMSO (39.52 ppm) and methanol (49.00 ppm) for ^{13}C NMR[5]. Data are reported as follows: chemical shifts (δ), multiplicity (br = broad, s = singlet, d = doublet, t = triplet, q = quartet, m = multiplet); coupling constant(s) (*J*) in Hz; integration. Unless otherwise noted, NMR data were collected at 25 °C. **Flash column chromatography:** Was performed using a Biotage SP1 system fitted with a KP-SIL SNAP Silica Gel (60 Å mesh) Flash Cartridge (FSKO-1107). **Purity determination:** Was conducted by UV absorbance at 254 nm during tandem liquid chromatography/mass spectrometry (LCMS) using a Waters Acquity separations module. **Identity**: Was determined via low-resolution mass spectrometry (LRMS) conducted in positive ion mode using a Waters Acquity SQD mass spectrometer (electrospray ionization source) fitted with a PDA detector. Mobile phase A consisted of 0.1% formic acid in water, while mobile phase B consisted of 0.1% formic acid in acetonitrile.

The gradient that was followed is presented in the table:

Time (min)	Flow (mL/min)	%A	%B
initial	0.4	90	10
1.8	0.4	5	95
2.3	0.4	5	95
2.5	0.4	90	10
3	0.4	90	10
5	0	90	10

Column 1: Acquity UPLC CSH C18 (2.1 x 50 mm, 130Å, 1.7 µm. Part No. 186005296) or Column 2: Acquity UPLC BEH C8 (2.1 x 50 mm, 130Å, 1.7 µm. Part No. 186002877) and were used with column temperature maintained at 25 °C. The sample solution injection volume was 1 µL. **Analytical thin-layer chromatography (TLC):** Was performed on aluminum sheets, silica gel 60 F_{254} (0.2 mm, VWR International, Darmstadt, Germany). Visualization was accomplished with UV light and aqueous potassium permanganate ($KMnO_4$) stain followed by heating. **High-resolution mass spectrometry (HRMS):** Was conducted using a Waters Xevo quadrupole-time-of-flight (QTOF) hybrid mass spectrometer system coupled with an Acquity ultra-performance liquid chromatography (UPLC) system. **Chromatographic separations**: Were carried out on an Acquity UPLC CSH C18 (2.1 x 50 mm, 130Å, 1.7 µm. Part No. 186005296) or Column 2: Acquity UPLC BEH C8 (2.1 x 50 mm, 130Å, 1.7 µm. Part No. 186002877). The mobile phase was 0.1% formic acid in water (solvent A) and 0.1% formic acid in acetonitrile (solvent B). Leucine Enkephalin was used as lock mass. MassLynx 4.1 was used for data analysis.

Procedure for the Preparation of OICR-9429(1)

<u>OICR-9429:</u> N-(4-(4-Methylpiperazin-1-yl)-3'-(morpholinomethyl)-[1,1'-biphenyl]-3-yl)-6-oxo-4-(trifluoromethyl)-1,6-dihydropyridine-3-carboxamide(1)

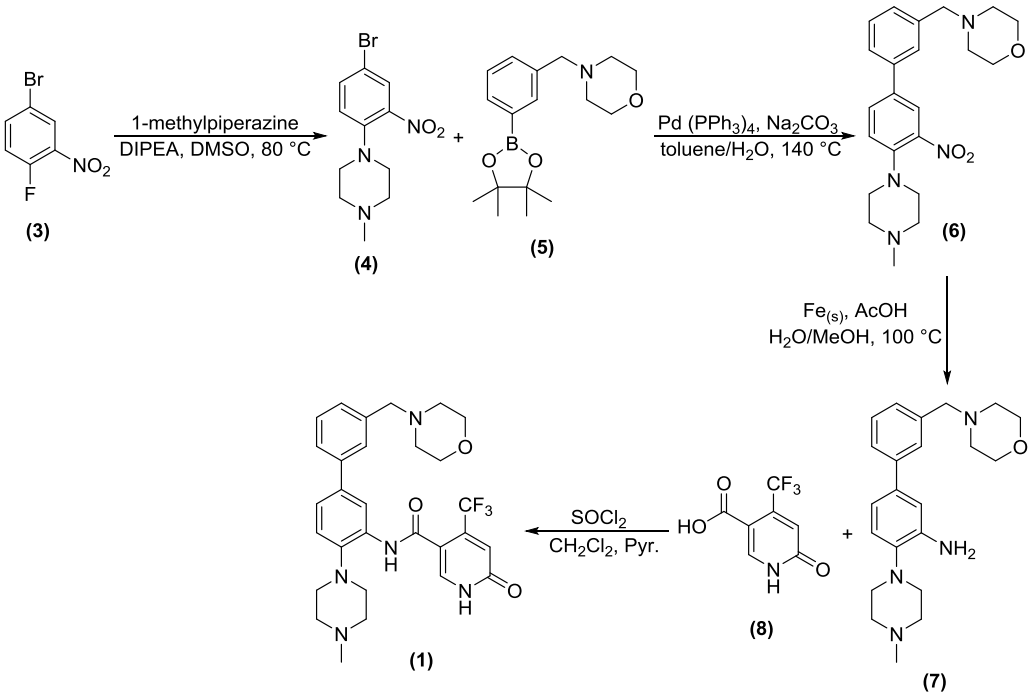

1-(4-Bromo-2-nitrophenyl)-4-methylpiperazine (4)

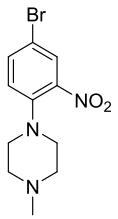

A 100 mL round bottom flask was charged with 4-bromo-1-fluoro-2-nitrobenzene **(3)** (3.4 mL, 27 mmol), 1-methylpiperazine (3.3 mL, 29 mmol), and *N,N*-diisopropylethylamine (9.2 mL, 54 mmol) in DMSO (20 mL). After 2 h at 80 °C the reaction mixture was diluted with water (50 mL) and EtOAc (50 mL), and the aqueous layer was extracted with EtOAc (3 x 50 mL). The combined organic layers were dried over $MgSO_4$, filtered, and concentrated under reduced pressure. The residue was purified by flash column chromatography (5-30% MeOH/EtOAc) to afford 1-(4-bromo-2-nitrophenyl)-4-methylpiperazine **(4)** (7.94 g, quantitative yield). ^{1}H NMR (500 MHz, DMSO-d_6) δ 8.00 (d, *J* = 2.4 Hz, 1H), 7.72 (dd, *J* = 2.4, 8.9 Hz, 1H), 7.26 (d, *J* = 8.9 Hz, 1H), 2.97 (t, *J* = 5.0 Hz, 4H), 2.40 (t, *J* = 4.8 Hz,

4H), 2.20 (s, 3H); ^{13}C NMR (125 MHz, DMSO-d_6) δ 144.3, 142.9, 136.2, 127.6, 123.4, 112.1, 54.3 (2), 50.8 (2), 45.6. HRMS (ESI) *m/z* calcd for $C_{11}H_{15}BrN_3O_2$ $[M+H]^+$: 300.0348, found: 300.0353.

4-((4'-(4-Methylpiperazin-1-yl)-3'-nitro-[1,1'-biphenyl]-3-yl)methyl)morpholine (6)

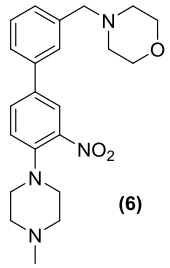

(6)

A microwave reaction vial was charged with 1-(4-bromo-2-nitrophenyl)-4-methylpiperazine **(4)** (757 mg, 2.52 mmol), 4-(3-(4,4,5,5-tetramethyl-1,3,2-dioxaborolan-2-yl)benzyl)morpholine **(5)** (1.00 g, 3.28 mmol), sodium carbonate (1.34 g, 12.6 mmol), $Pd(Ph_3P)_4$ (291 mg, 0.252 mmol) and toluene/water (1:1, 6 mL). The reaction mixture was then heated to 140 °C for 1 h in a microwave. After being cooled down to room temperature, the solution was then diluted with EtOAc (10 mL) and water (10 mL), and the aqueous layer extracted with EtOAc (3 x 10 mL). The combined organic layers were then dried over anhydrous $MgSO_4$, filtered and concentrated under reduced pressure. The crude product was purified by silica gel flash column chromatography (5-50 % MeOH/EtOAc) to afford 4-((4'-(4-Methylpiperazin-1-yl)-3'-nitro-[1,1'-biphenyl]-3-yl)methyl)morpholine **(6)** (772 mg, 77%). ^{1}H NMR (500 MHz, DMSO-d_6) δ 8.07 (s, 1H), 7.88 (d, *J* = 8.5 Hz, 1H), 7.60 (s, 1H), 7.58 (d, *J* = 8.0 Hz, 1H), 7.43 (t, *J* = 7.5 Hz, 1H), 7.39 (d, *J* = 8.5 Hz, 1H), 7.33 (d, *J* = 7.5 Hz, 1H), 3.58 (t, *J* = 4.0 Hz, 4H), 3.54 (s, 2H), 3.04 (t, *J* = 4.5 Hz, 4H), 2.45 (t, *J* = 4.0 Hz, 4H), 2.39 (t, *J* = 4.0 Hz, 4H), 2.24 (s, 3H); ^{13}C NMR (125 MHz, DMSO-d_6) δ 144.7, 143.5, 139.2, 138.1, 133.8, 131.9, 129.5, 128.9, 127.4, 125.5, 123.6, 122.3, 66.7 (2C), 62.8, 55.0 (2), 53.7 (2), 51.4 (2), 46.2. HRMS (ESI) *m/z* calcd for $C_{22}H_{29}N_4O_3$ $[M+H]^+$: 397.2240, found: 397.2238.

4-(4-Methylpiperazin-1-yl)-3'-(morpholinomethyl)-[1,1'-biphenyl]-3-amine (7)

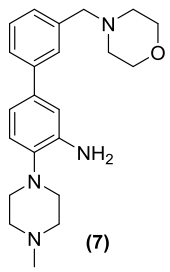

(7)

4-((4'-(4-Methylpiperazin-1-yl)-3'-nitro-[1,1'-biphenyl]-3-yl)methyl)morpholine **(6)** (772 mg, 1.95 mmol), iron powder (653 mg, 11.7 mmol), and glacial acetic acid (0.56 mL, 9.75 mmol) were dissolved in a mixture of MeOH (20 mL) and water (4 mL), and refluxed at 100 °C for 2 h. The solution was then

basified with 1M NaOH to pH = 11, diluted with brine, and extracted with EtOAc (5 x 50 mL). The combined organic layers were dried over $MgSO_4$, filtered, and concentrated under reduced pressure. The crude product was purified by flash column chromatography (5-50% MeOH/EtOAc) to afford 4-(4-methylpiperazin-1-yl)-3'-(morpholinomethyl)-[1,1'-biphenyl]-3-amine **(7)** (620 mg, 87% yield). HRMS (ESI) *m/z* calcd for $C_{22}H_{31}N_4O$ $[M+H]^+$: 366.2412, found: 366.2409.

N-(4-(4-Methylpiperazin-1-yl)-3'-(morpholinomethyl)-[1,1'-biphenyl]-3-yl)-6-oxo-4-(trifluoromethyl)-1,6-dihydropyridine-3-carboxamide (OICR-9429) (1)

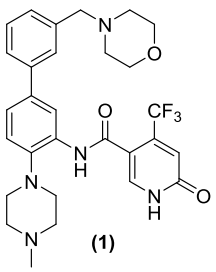

(1)

6-Hydroxy-4-(trifluoromethyl)nicotinic acid **(8)** (462 mg, 2.23 mmol) was suspended in $SOCl_2$ (6 mL) and stirred at 70 °C for 2 h until the solution went clear. Excess $SOCl_2$ was then removed under reduced pressure, and the residue dried under high vacuum for 1 h. The dried residue was subsequently dissolved in CH_2Cl_2 (10 mL), and added dropwise to a solution of 4-(4-methylpiperazin-1-yl)-3'-(morpholinomethyl)-[1,1'-biphenyl]-3-amine **(7)** (680 mg, 1.86 mmol) and pyridine (0.21 mL, 2.60 mmol) in CH_2Cl_2 (5 mL). After 2 h, the reaction mixture was diluted with saturated aqueous sodium bicarbonate solution (20 mL) and extracted with EtOAc (3 x 20 mL). The combined organic extracts were dried over anhydrous $MgSO_4$, filtered, and concentrated under reduced pressure. The residue was purified by silica gel flash column chromatography (5-40% MeOH/EtOAc) to afford *N*-(4-(4-methylpiperazin-1-yl)-3'-(morpholinomethyl)-[1,1'-biphenyl]-3-yl)-6-oxo-4-(trifluoromethyl)-1,6-dihydropyridine-3-carboxamide **(1)** (207 mg, 20%). ^{1}H NMR (500 MHz, DMSO-d_6) δ 8.25 (s, 1H), 7.99 (s, 1H), 7.61 (s, 1H), 7.54 (d, *J* = 7.7 Hz, 1H), 7.47 (dd, *J* = 1.6, 8.3 Hz, 1H), 7.40 (t, *J* = 7.6 Hz, 1H), 7.27-7.37 (m, 2H), 6.92 (s, 1H), 3.70 (t, *J* = 4.5 Hz, 4H), 3.54-3.65 (m, 2H), 3.02 (t, *J* = 4.6 Hz, 4H), 2.74 (br s, 4H), 2.51 (br. s., 4H), 2.42 (s, 3H); ^{13}C NMR (125 MHz, DMSO-d_6) δ 163.6, 162.9, 143.2, 140.4, 140.0 (d, $^2J_{C\text{-}F}$ = 33.6 Hz, 1C), 138.4, 137.5, 137.4, 132.4, 128.5, 128.3, 127.7, 125.6, 124.1, 121.2, 120.7, 119.0 (q, $^3J_{C\text{-}F}$ = 5.5 Hz, 1C), 122.0 (q, $^1J_{C\text{-}F}$ = 274.6 Hz, 1C), 113.3, 66.3, 62.9, 54.8 (2), 53.2, 51.0 (2), 44.4. HRMS (ESI) *m/z* calcd for $C_{29}H_{33}F_3N_5O_3$ $[M+H]^+$: 556.2535, found: 556.2526.

Procedure for the Preparation of OICR-0547(2)

<u>OICR-0547:</u> N-(4-morpholino-3'-(morpholinomethyl)biphenyl-3-yl)-6-oxo-4-(trifluoromethyl)-1,6-dihydropyridine-3-carboxamide (2)

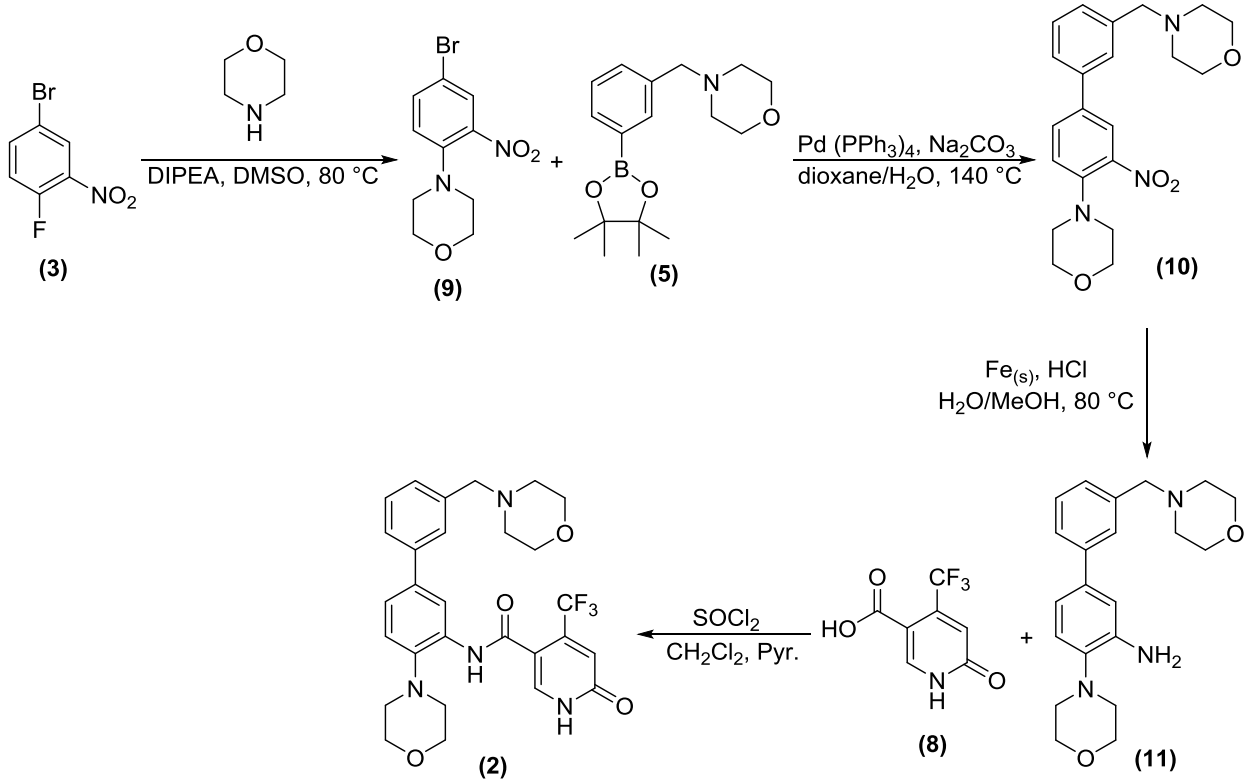

4-(4-bromo-2-nitrophenyl)morpholine (9)

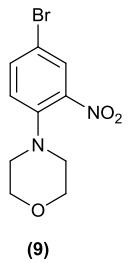
(9)

A 100 mL round bottom flask was charged with 4-bromo-1-fluoro-2-nitrobenzene **(3)** (2.80 ml, 22.32 mmol), morpholine (2.118 ml, 24.55 mmol, 1.1 equiv), and *N,N*-diisopropylethylamine (7.67 ml, 44.6 mmol, 2.0 equiv) in DMSO (13 mL). The reaction turned red and was stirred for 3 h at 80-85 °C. The reaction mixture was diluted with water (60 mL) and the aqueous layer was extracted with CH_2Cl_2 (3 x 50 mL). The combined organic layers were dried over Na_2SO_4, filtered, and concentrated under reduced pressure. The product was isolated as an orange oil and was used in the nest step without further purification.

Analysis of the crude compound showed:

Yield: 90% (7.08 g); **^{1}H NMR** (500 MHz, $CDCl_3$) δ 7.90 (d, *J* = 2.3 Hz, 1H), 7.58 (dd, *J* = 8.8, 2.4 Hz, 1H), 7.03 (d, *J* = 8.8 Hz, 1H), 3.83 – 3.81 (m, 4H), 3.04 – 3.02 (m, 4H); **^{13}C NMR** (126 MHz, $CDCl_3$) δ 145.00, 143.85, 136.54, 128.74, 122.62, 114.13, 66.82, 52.08; **LRMS** (ESI): 287.17 (97.3%), 289.18 (100%); **UPLC**: τ = 6.9 min, column 1.

4-((4'-morpholino-3'-nitrobiphenyl-3-yl)methyl)morpholine (10)

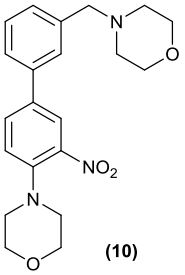

(10)

A microwave reaction vial was charged with 4-(4-bromo-2-nitrophenyl)morpholine **(9)** (2.0 g, 5.65 mmol), 4-(3-(4,4,5,5-tetramethyl-1,3,2-dioxaborolan-2-yl)benzyl)morpholine **(5)** (2.21 g, 7.06 mmol, 1.25 equiv), sodium carbonate, anhydrous (2.99 g, 28.2 mmol, 5.0 equiv), $Pd(PPh_3)_4$ (0.653 g, 0.565 mmol, 0.1 equiv) and dioxane/water (1:1, 14 mL). The reaction mixture was then irradiated to 140 °C for 1.5 h in a microwave. After being cooled down to room temperature, the solution was then concentrated under reduced pressure to approx. 5-7 mL. Water (10 mL) and CH_2Cl_2 (10 mL) were added to the suspension, the organic layer was separated and the aqueous layer was extracted with CH_2Cl_2 (3 x 10 mL). *Note: Sonication for 10 min was required to dissolve the white precipitate.* The combined organic layers were then dried over anhydrous Na_2SO_4, filtered, and concentrated under reduced pressure. The crude product was purified by silica gel flash column chromatography (Gradient: 100% to 60%, CH_2Cl_2 : 89% CH_2Cl_2, 10% MeOH, 1% NH_4Ac; during 40 min using KP-SIL 50 g column, product was collected at 80% of the mixture) to yield the desired product 4-((4'-morpholino-3'-nitro-[1,1'-biphenyl]-3-yl)methyl)morpholine **(10)** (2.62 g, 4.33 mmol, 77 % yield) as a red oil.

Analysis of the purified compound showed:

Yield: 77% (2.62 g); **^{1}H NMR** (500 MHz, MeOD) δ 8.04 (d, J = 2.2 Hz, 1H), 7.86 (dd, J = 8.6, 2.2 Hz, 1H), 7.70 (s, 1H), 7.62 (d, J = 7.7 Hz, 1H), 7.48 (t, J = 7.6 Hz, 1H), 7.41 (d, J = 7.6 Hz, 1H), 7.38 (d, J = 8.6 Hz, 1H), 3.85 (s, 2H), 3.83 – 3.79 (m, 5H), 3.79 – 3.74 (m, 4H), 3.09 – 3.06 (m, 4H), 2.75 (s, 4H); **^{13}C NMR** (126 MHz, MeOD) δ 146.03, 145.66, 140.17, 136.26, 132.73, 130.70, 130.46, 129.40, 127.58, 124.60, 123.05, 67.95, 66.86, 63.53, 54.16, 53.23; **LRMS** (ESI): 384.30; **UPLC**: τ = 0.95 min, column 1.

4-morpholino-3'-(morpholinomethyl)biphenyl-3-amine (11)

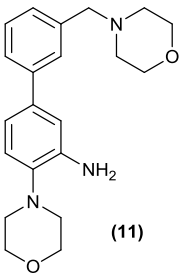

(11)

In a 100 mL flask 4-((4'-morpholino-3'-nitro-[1,1'-biphenyl]-3-yl)methyl)morpholine **(10)** (2.62 g, 4.33 mmol), iron powder (1.210 g, 21.66 mmol, 5.0 equiv) and hydrochloric acid (0.036 ml, 0.433 mmol, 0.1 equiv) were dissolved in methanol/water (1:1, 10 mL) and heated at 80-90 °C for 3 h. *Note 1: the stirring was set to the maximum possible to avoid clump formation. Note 2: the product decomposes at high temperature, do not exceed 90* °C*.* The solution was filtered through celite, and rinsed with CH_2Cl_2 (2 X 15 mL). The brown solution was then basified with 1M NaOH to pH = 11-10, diluted with brine, and extracted with CH_2Cl_2 (5 x 30 mL). The combined organic layers were dried over $MgSO_4$, filtered, and concentrated under reduced pressure. *Note 3: concentration under reduced pressure was performed by rotary evaporation at 30 °C.* The crude product was purified by flash column chromatography (Gradient: 100% to 50%, CH_2Cl_2 : 89% CH_2Cl_2, 10% MeOH, 1% NH_4Ac; during 60 min using KP-SIL 50 g column, product was collected at 70% of the mixture) to afford 982.22 mg of a white solid.

Analysis of the purified compound showed:

Yield: 57.3% yield (0.982 g); **^{1}H NMR** (500 MHz, CDCl3) δ 7.60 (dd, J = 12.0, 7.2 Hz, 3H), 7.47 (td, J = 7.4, 1.1 Hz, 2H), 7.39 (td, J = 7.5, 2.7 Hz, 4H), 7.28 (t, J = 7.5 Hz, 1H), 6.99 (d, J = 8.2 Hz, 1H), 6.95 – 6.89 (m, 2H), 3.98 (s, 2H), 3.83 – 3.76 (m, 4H), 3.65 (s, 4H), 3.48 (s, 2H), 2.93 – 2.85 (m, 4H), 2.40 (s, 4H); **^{13}C NMR** (126 MHz, CDCl3) δ 141.82, 138.59, 133.19, 132.37, 132.29, 132.21, 132.06, 132.04, 128.71, 128.68, 128.58, 127.97, 120.16, 117.71, 114.13, 67.81, 67.14, 63.66, 53.77, 51.68; **LRMS** (ESI): 354.46; UPLC: τ = 0.78 min, column 1.

N-(4-morpholino-3'-(morpholinomethyl)biphenyl-3-yl)-6-oxo-4-(trifluoromethyl)-1,6-dihydropyridine-3-carboxamide (2)

*Note 1: Prior to the experiment, 6-Hydroxy-4-(trifluoromethyl)nicotinic acid **(8)** and **(11)** were dried under high vacuum for 24 h.*

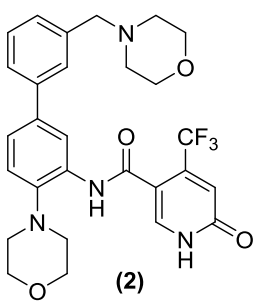

(2)

The 6-hydroxy-4-(trifluoromethyl)nicotinic acid **(8)** (0.617 g, 2.98 mmol, 1.2 equiv) was suspended in $SOCl_2$ (8.10 ml, 112 mmol, 45 equiv) to form a white slurry. The slurry was stirred at 70 °C for 2 h until the solution went clear. The remaining $SOCl_2$ was removed under reduced pressure, and the residue dried under high vacuum for 1 h. *Note 2: A trap filled with KOH was used to neutralize the HCl_{gas} generated.* The dried residue was subsequently dissolved in CH_2Cl_{2anhyd} (10 mL), and added drop wise over 20-30 min to a solution of **11** (0.98222 g, 2.481 mmol) and $pyridine_{anhyd}$ (0.300 ml, 3.72 mmol, 1.5 equiv) in CH_2Cl_2 (5 mL). After 16 h, the reaction mixture was diluted with saturated aqueous sodium bicarbonate solution (20 mL) and extracted with CH_2Cl_2 (3 x 20 mL) *Note 3: Sonication was necessary to dissolve the black solid formed.* The combined organic extracts were dried over anhydrous Na_2SO_4, filtered, and concentrated under reduced pressure. The residue was purified by silica gel flash column chromatography (Gradient: 70% to 20%, CH_2Cl_2 : 89% CH_2Cl_2, 10% MeOH, 1% NH4Ac; during 60 min using KP-SIL 50 g column, product was collected at 40% of the mixture, tailing was observed) to afford the title compound **(2)** as a white solid.

Analysis of the purified compound showed:

Yield: 8.57% yield (0.119 g); **^{1}H NMR** (500 MHz, MeOD) δ 8.26 (d, J = 1.2 Hz, 1H), 7.96 (s, 1H), 7.61 (s, 1H), 7.53 (d, J = 7.8 Hz, 1H), 7.46 (dd, J = 8.3, 2.0 Hz, 1H), 7.39 (t, J = 7.6 Hz, 1H), 7.33 - 7.28 (m, 2H), 6.92 (s, 1H), 3.84 - 3.81 (m, 4H), 3.70 - 3.67 (m, 4H), 3.58 (s, 2H), 2.95 - 2.90 (m, 4H), 2.49 (s, 4H); **^{13}C NMR** (126 MHz, MeOD) δ 164.90, 164.18, 144.81, 141.79, 141.39 (q, $J^{2}[^{13}C\text{-}^{19}F]$ = 33.2 Hz), 139.67, 138.87, 138.78, 133.85, 129.89, 129.66, 129.09, 126.99, 126.67, 125.44, 124.49, 123.40 (q, $J^{1}[^{13}C\text{-}^{19}F]$ = 274.6 Hz), 122.53, 122.04, 120.43 (q, $J^{3}[^{13}C\text{-}^{19}F]$ = 11.0, 5.6 Hz), 114.71, 68.23, 67.70, 64.29, 54.63, 53.58. **^{19}F NMR** (471 MHz, MeOD) δ -63.80; **LRMS** (ESI): 543.49; UPLC: τ = 0.92 min, column 2.